‘high resolution’ transmission electron microscopy image simulations

Robin Schäublin

Scientific Center for Optical and Electron Microscopy
&
Metal Physics and Technology
ETH Hönggerberg
CH-8093 Zürich

05.11.2024

Introduction

The dislocation

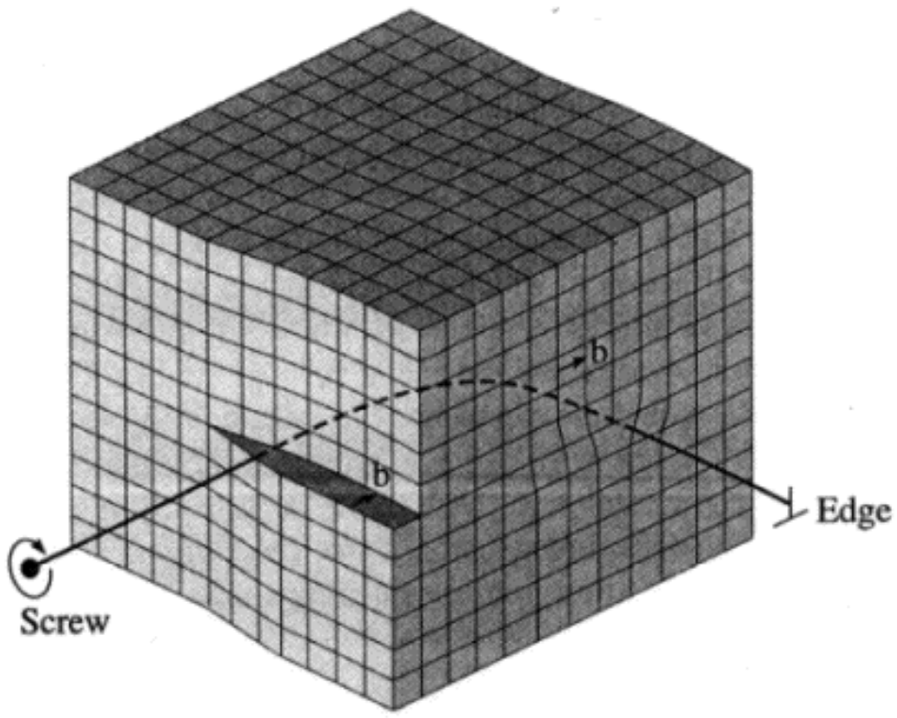

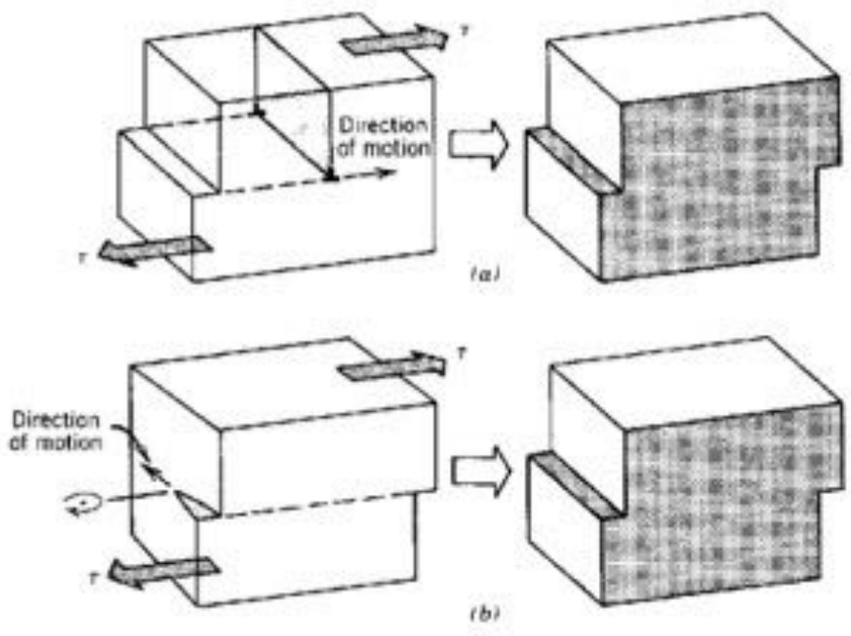

Edge Dislocation:

Dislocation moves in direction of applied shear stress

Screw Dislocation:

Dislocation motion is perpendicular to applied shear stress

Taylor, Polanyi and Orowan (**1934**): Plasticity occurs through the motion of dislocations 😊
Dislocation characterized by its **Burgers vector b**

W. T. Read : " *It became the fashion to invent a dislocation theory [for everything ...]* " **1954** 😰

First TEM observation of the dislocation: 1956 😅

P.B. Hirsch, R.W. Horne and M.J. Whelan, Phil. Mag. 1 677 (1956) ... *July*
W. Bollmann, Phys. Rev. 103 1588 (1956) *September.*

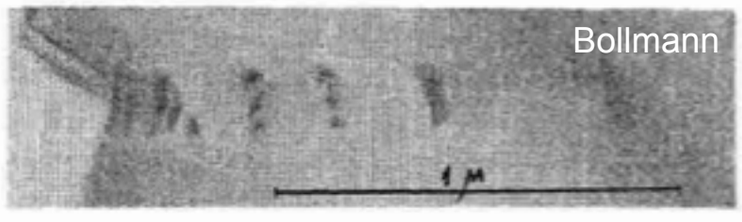

FIG. 1. Sections of dislocation lines crossing a steel foil.

Introduction

contrasts in transmission electron microscopy relate to three origins:

1) Absorption contrast (thickness, mass, Z)
2) Diffraction contrast (crystallography)
3) Phase contrast

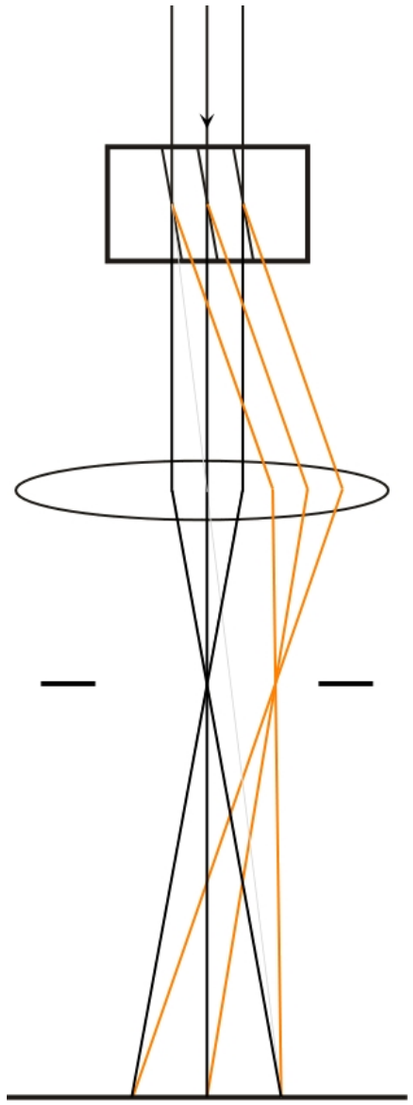

TEM no objective aperture

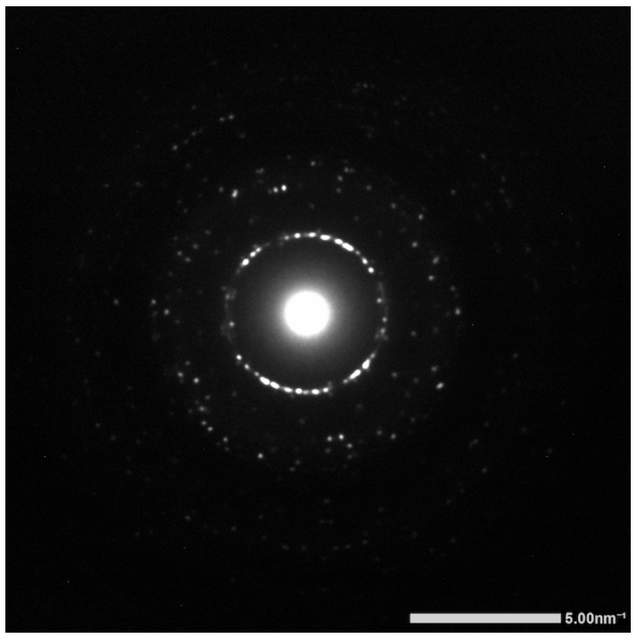

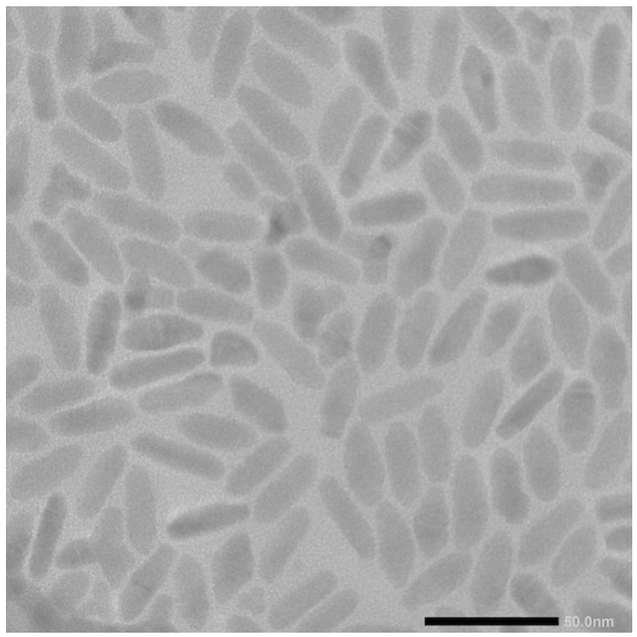

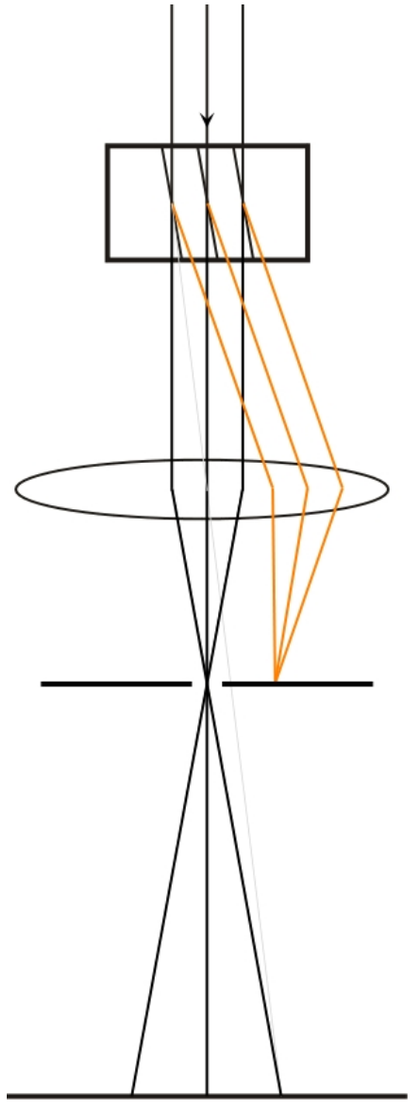

TEM bright field

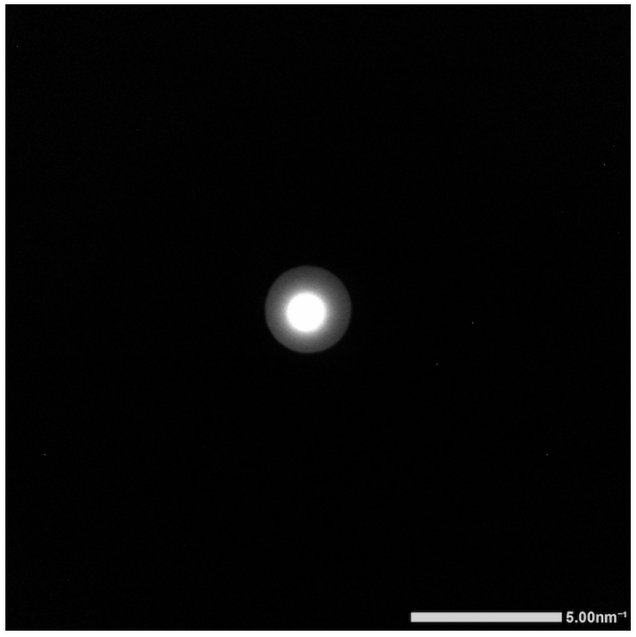

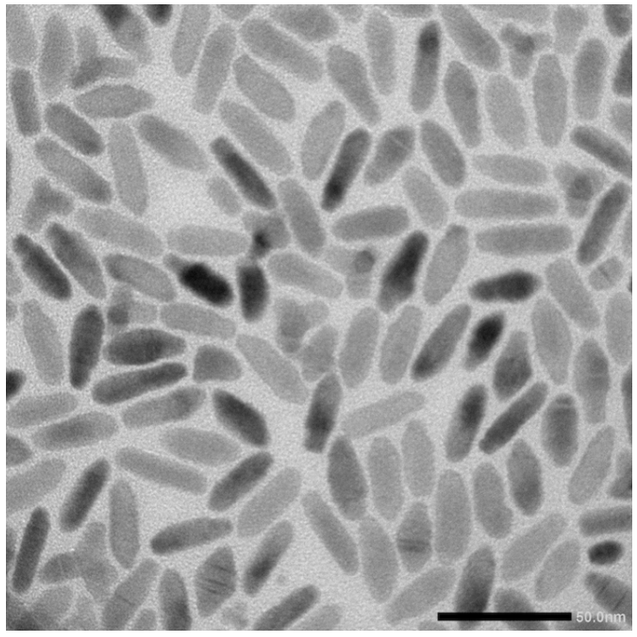

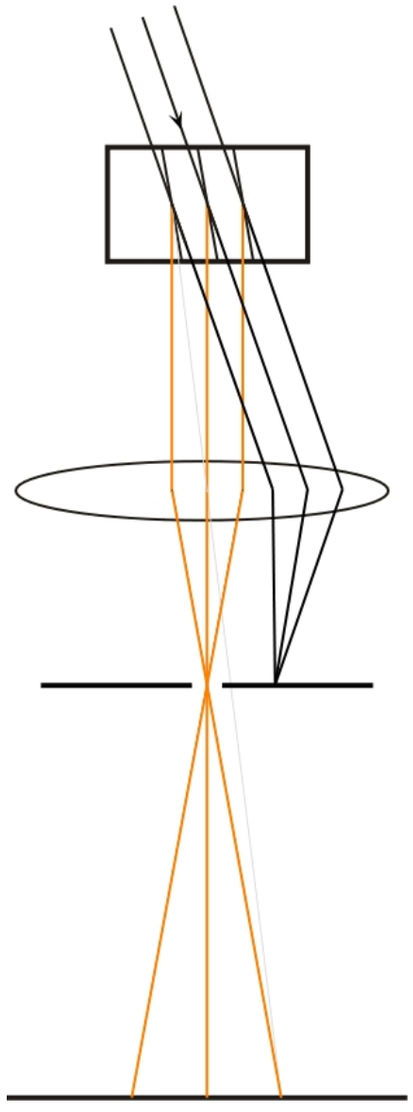

TEM dark field

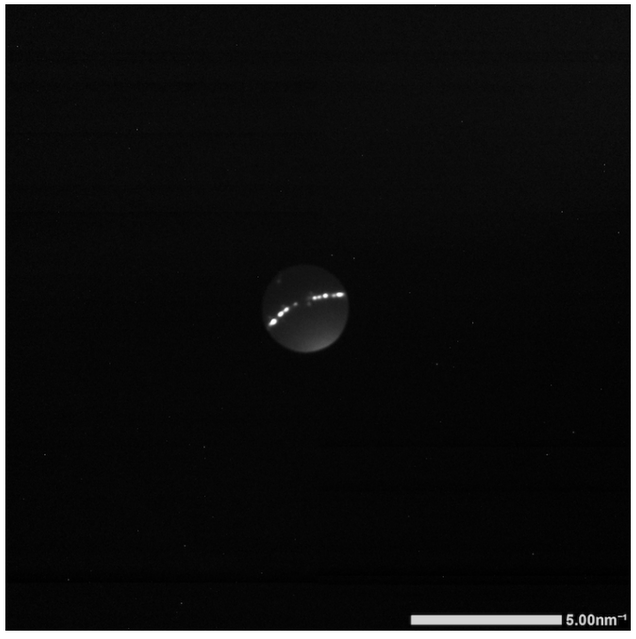

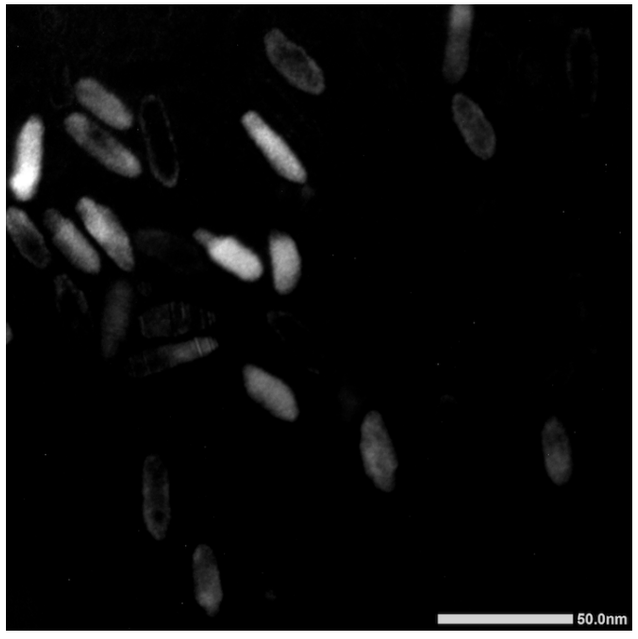

Diffraction pattern – no objective aperture

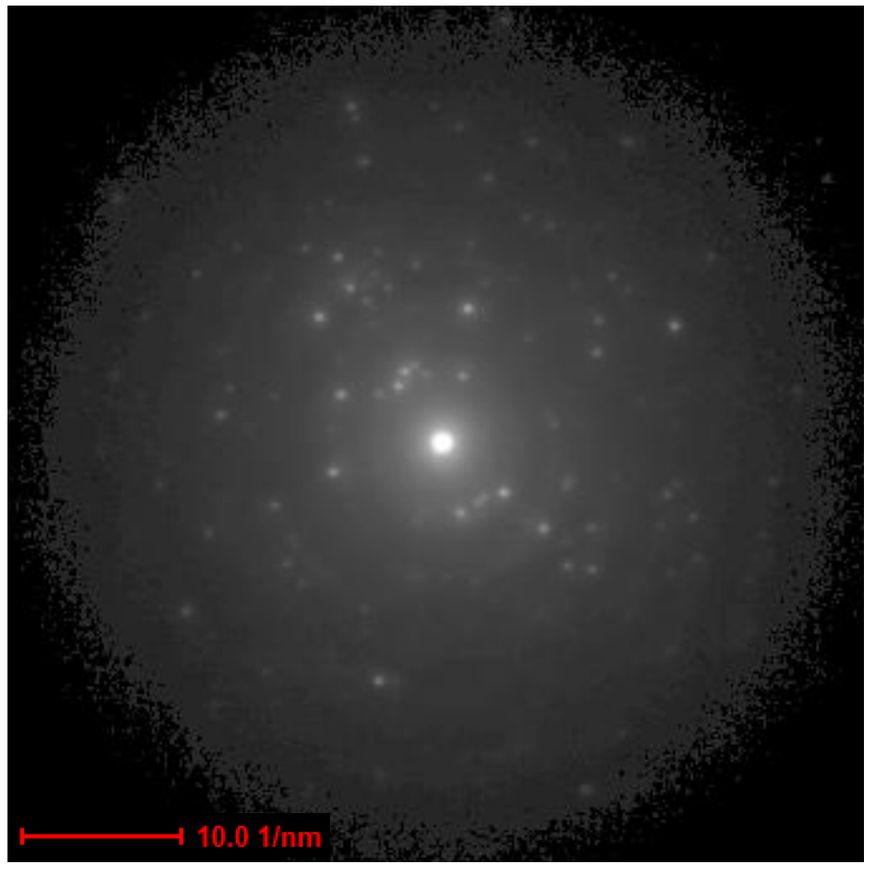

TEM image

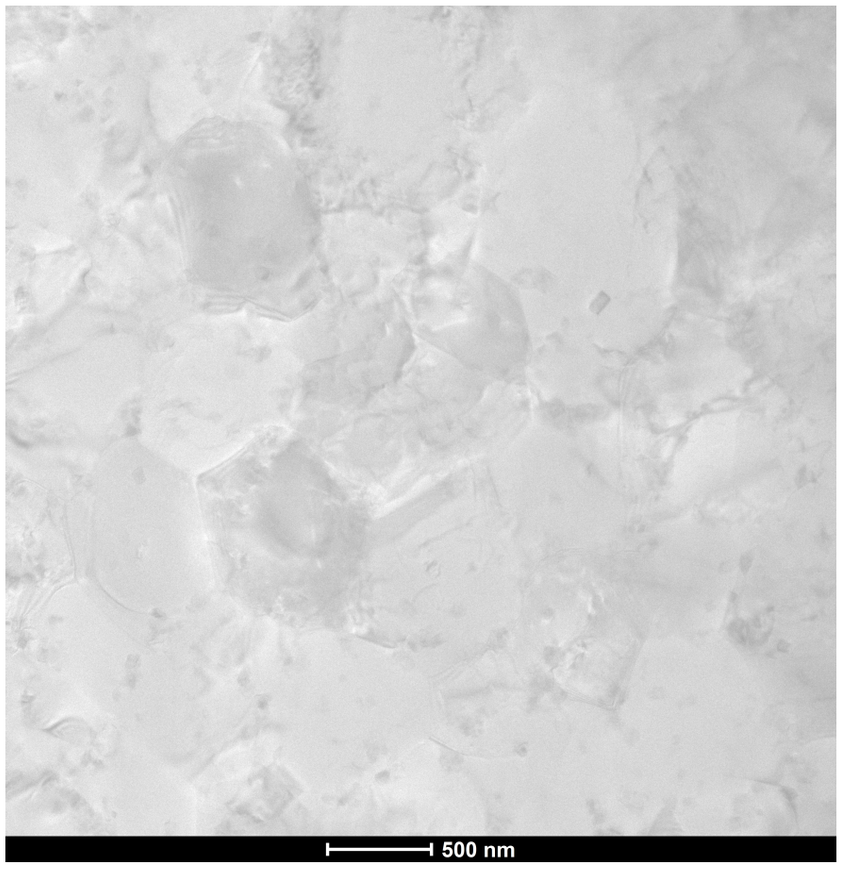

Diffraction pattern – bright field

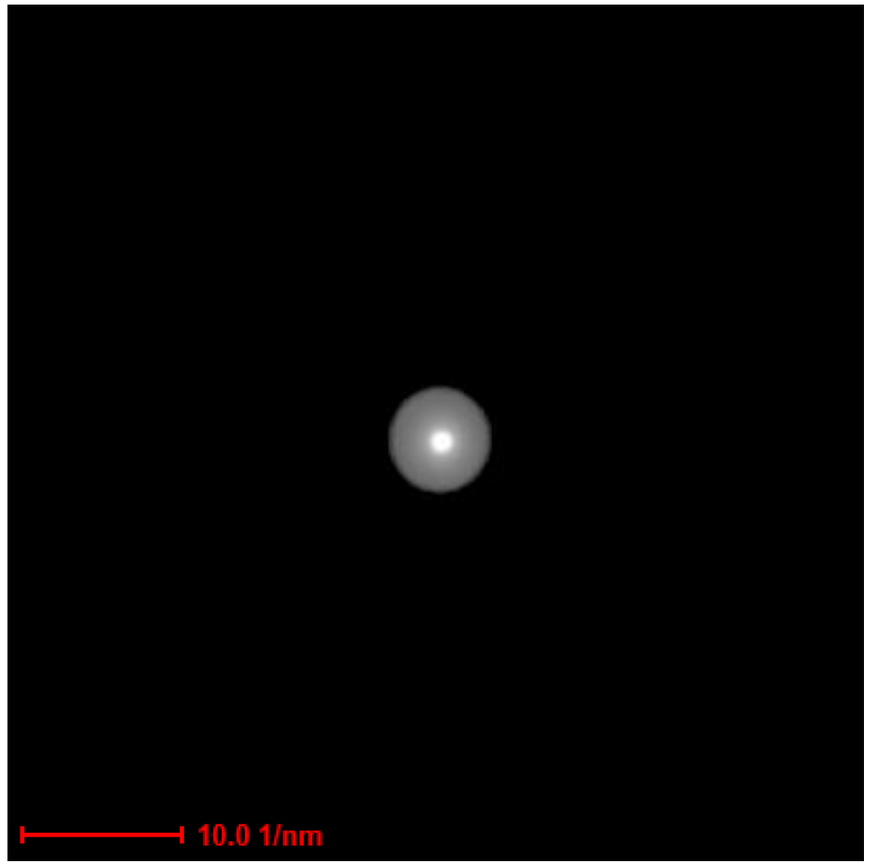

TEM image

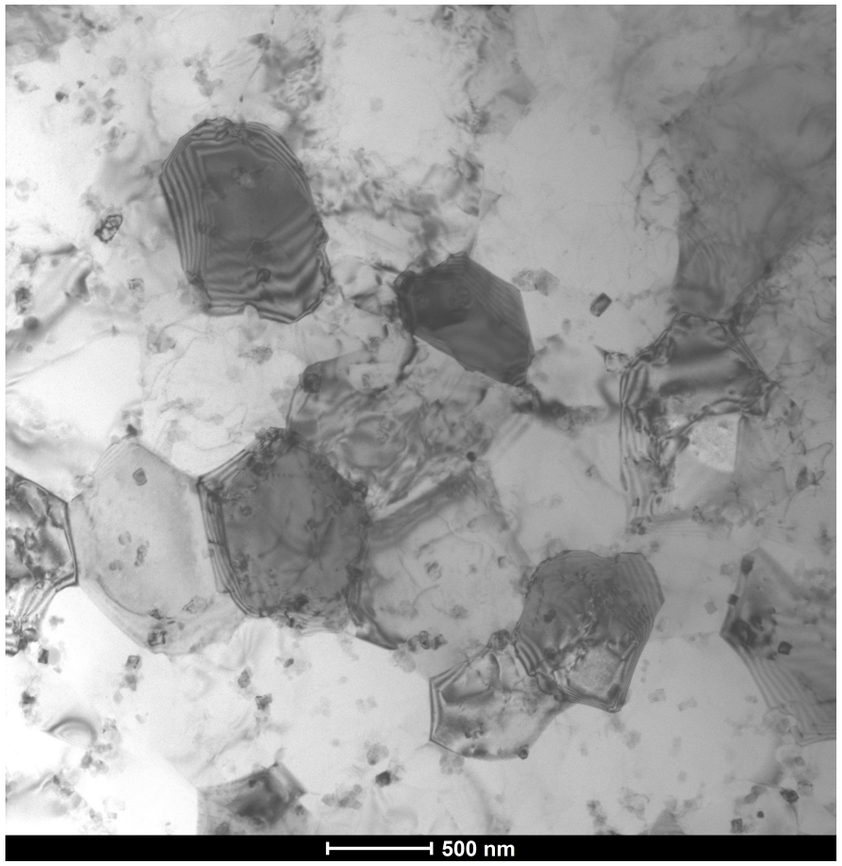

Diffraction pattern – dark field

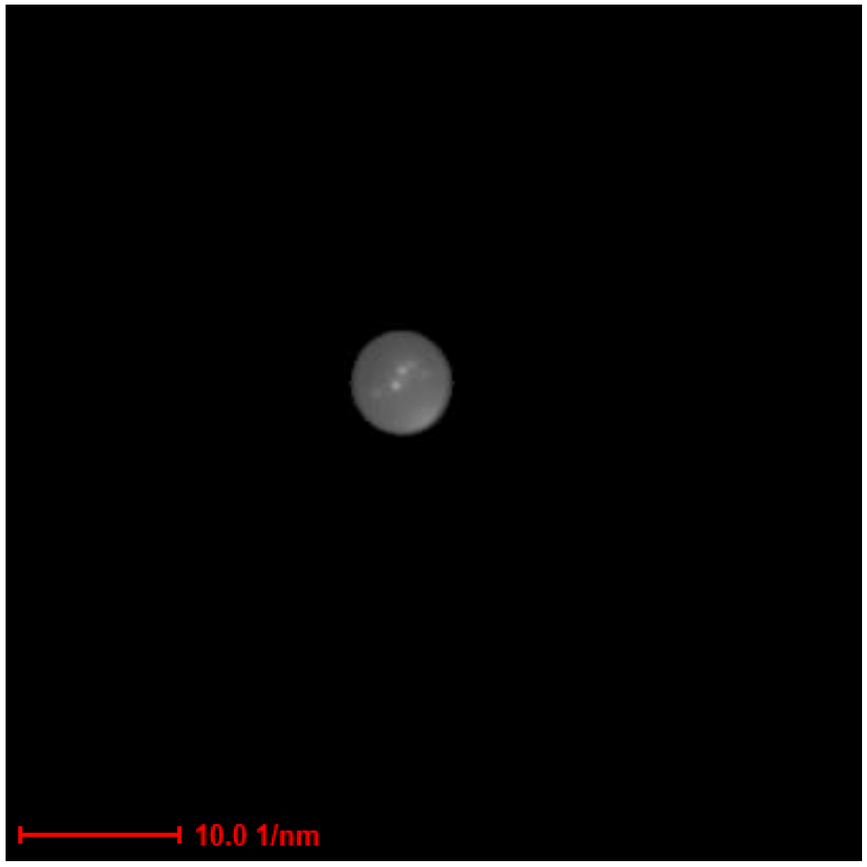

TEM image

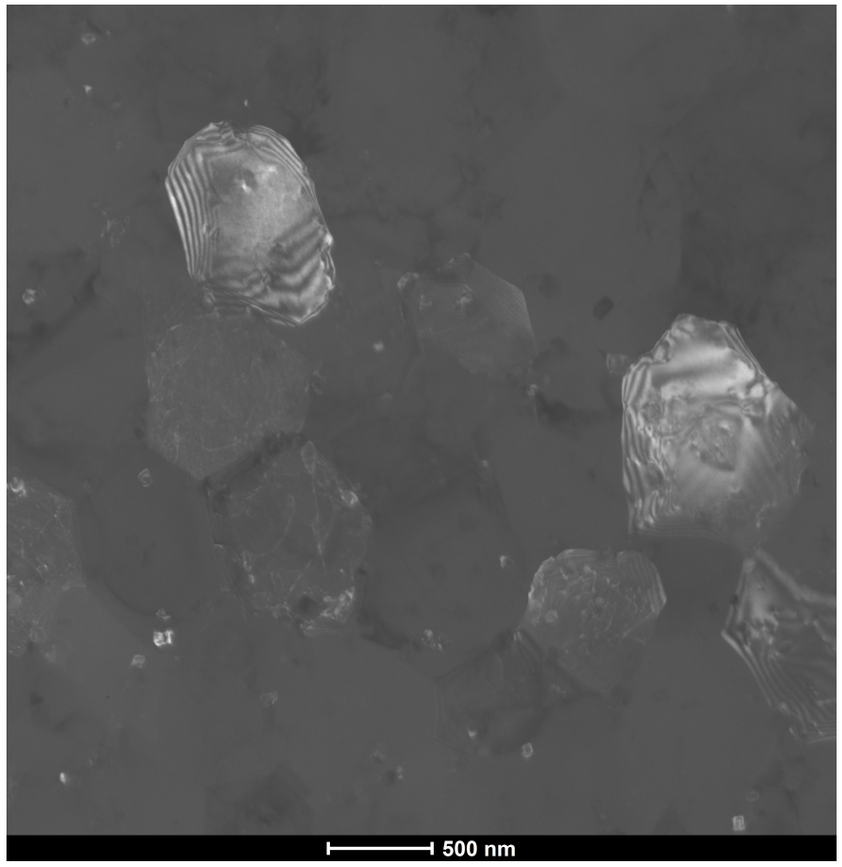

Motivation: *the future fusion reactor*

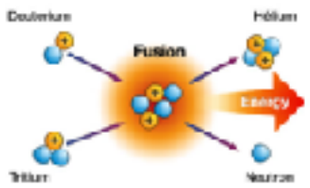

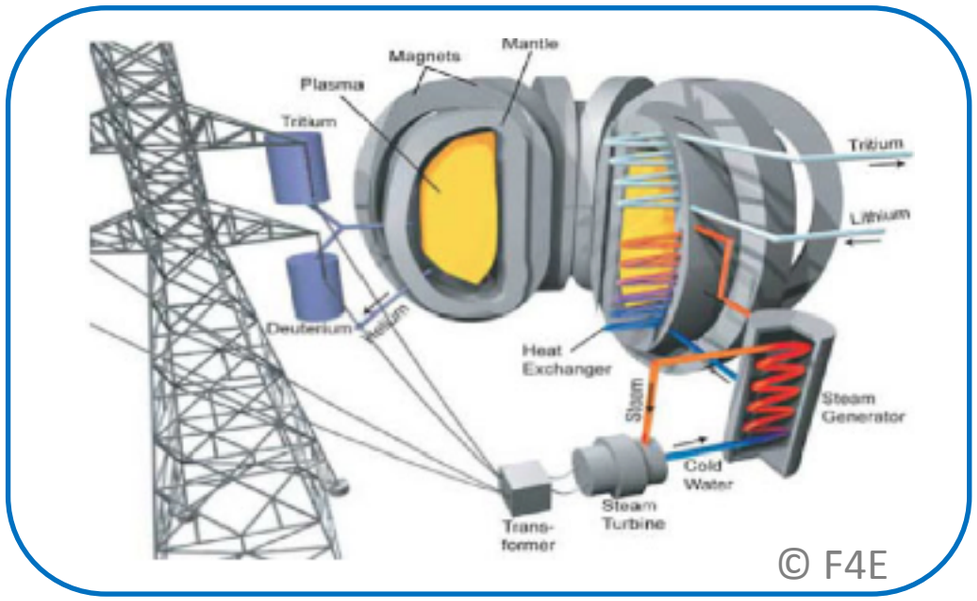

© F4E

irradiation of ferritic steel → hardening, loss of ductility:

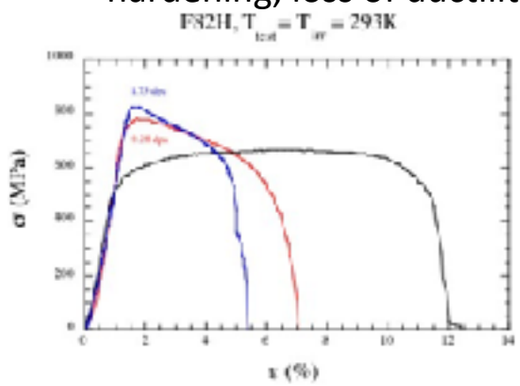

Spätig et al JNM 1998

14 MeV neutrons

- **Ferritic steels** are prime candidates for the plasma-facing wall of the **future fusion reactor**, for their resistance to radiation damage compared to e.g. stainless steels.
- However, they will suffer from large **irradiation doses** and **heat loads**, which change mechanical properties because of the induced **lattice defects** and **phase separation**.
- **Understanding** these **microstructural changes** is key for their safe application.
-

MOLECULAR DYNAMICS SIMULATIONS OF RADIATION DAMAGE THE DISPLACEMENT CASCADE

Au cube, pka 5 keV,
10 K
40 ps, 1 frame every
0.2 ps

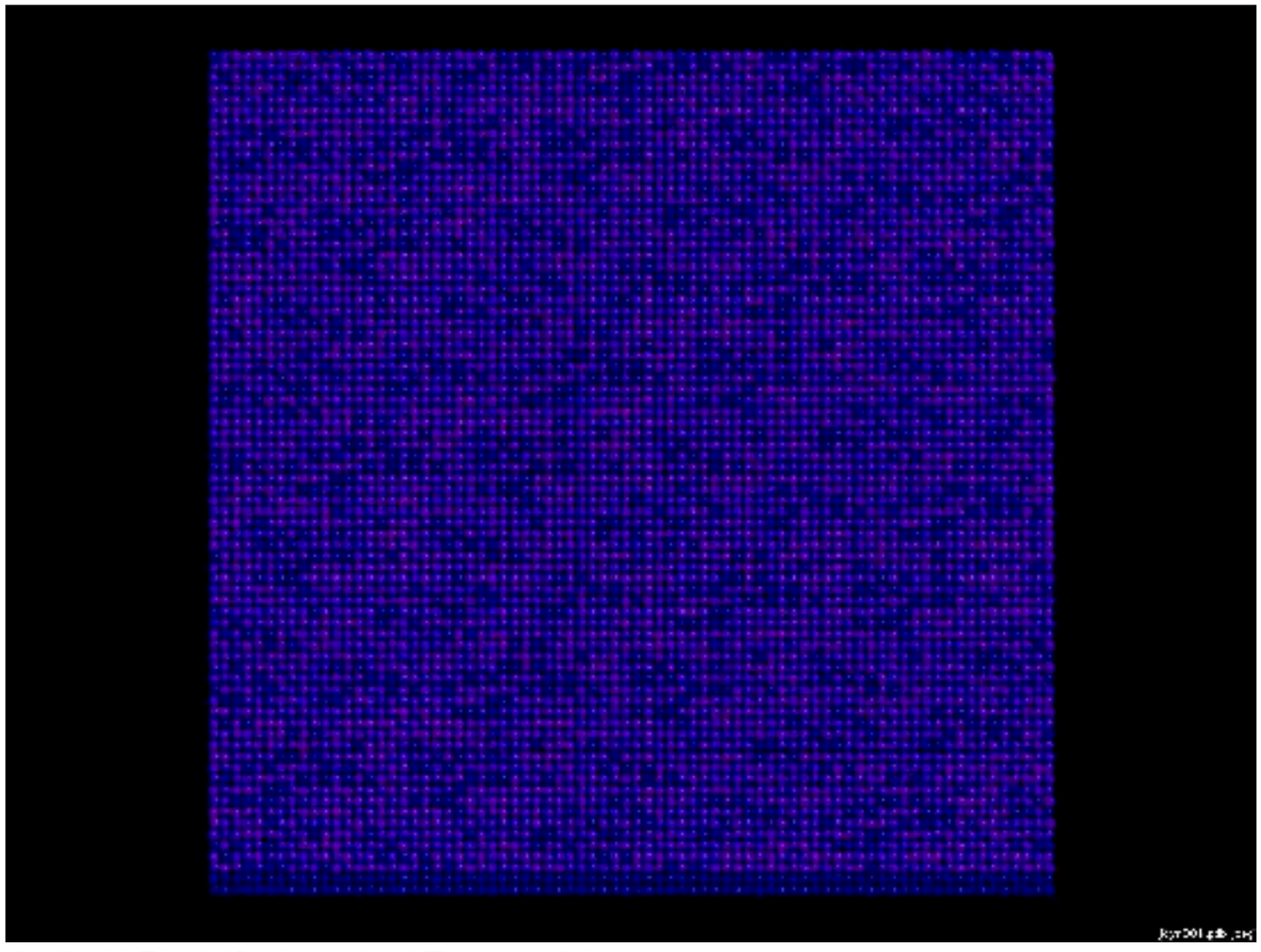

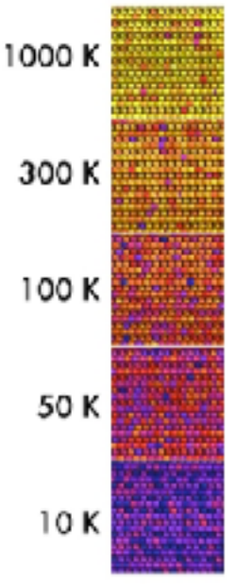

AuBulk5keV3, box is 15 nm wide

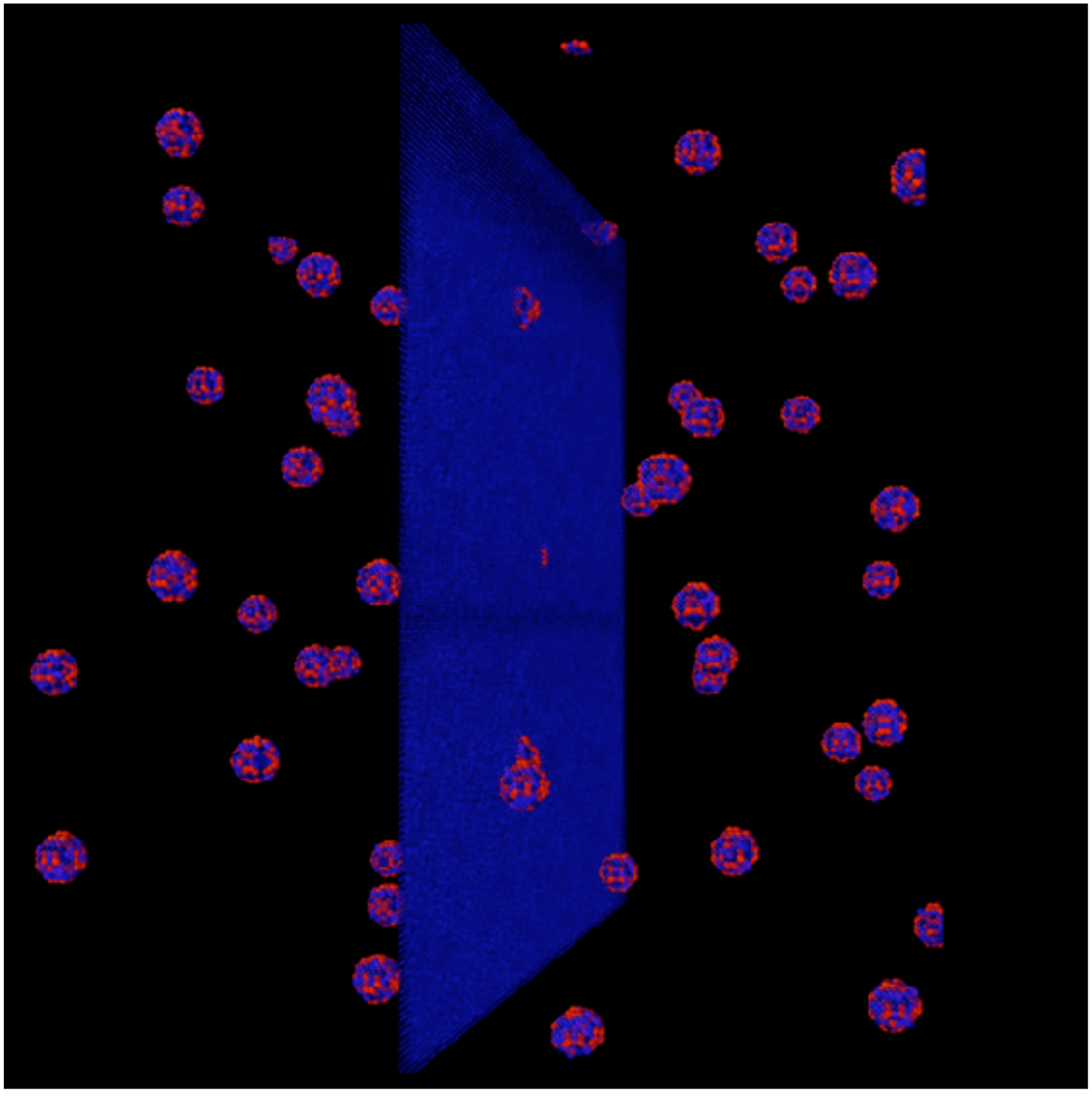

ETH zürich LMPT metal physics and technology

50 keV cascade in Fe(Cr) at 10 K

Molecular Dynamics simulation, *mdcask* code
Fe 150x150x150 unit cells -> 6.75 millions atoms
42.8^3 nm^3
pure Cr precipitates 2 nm in diameter
$1x10^{24}$ m^{-3} -> 53 precipitates, 11 nm between them
pka starts at 350 fs
colour depicts kinetic energy (temperature)

FinalRunEkin0 .02Slice

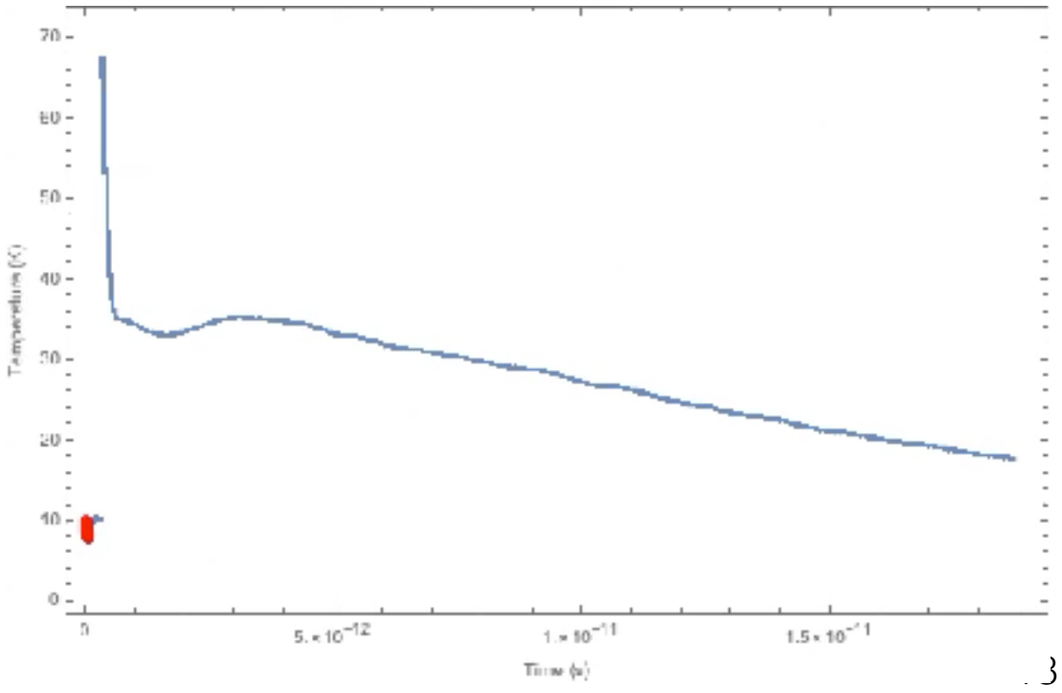

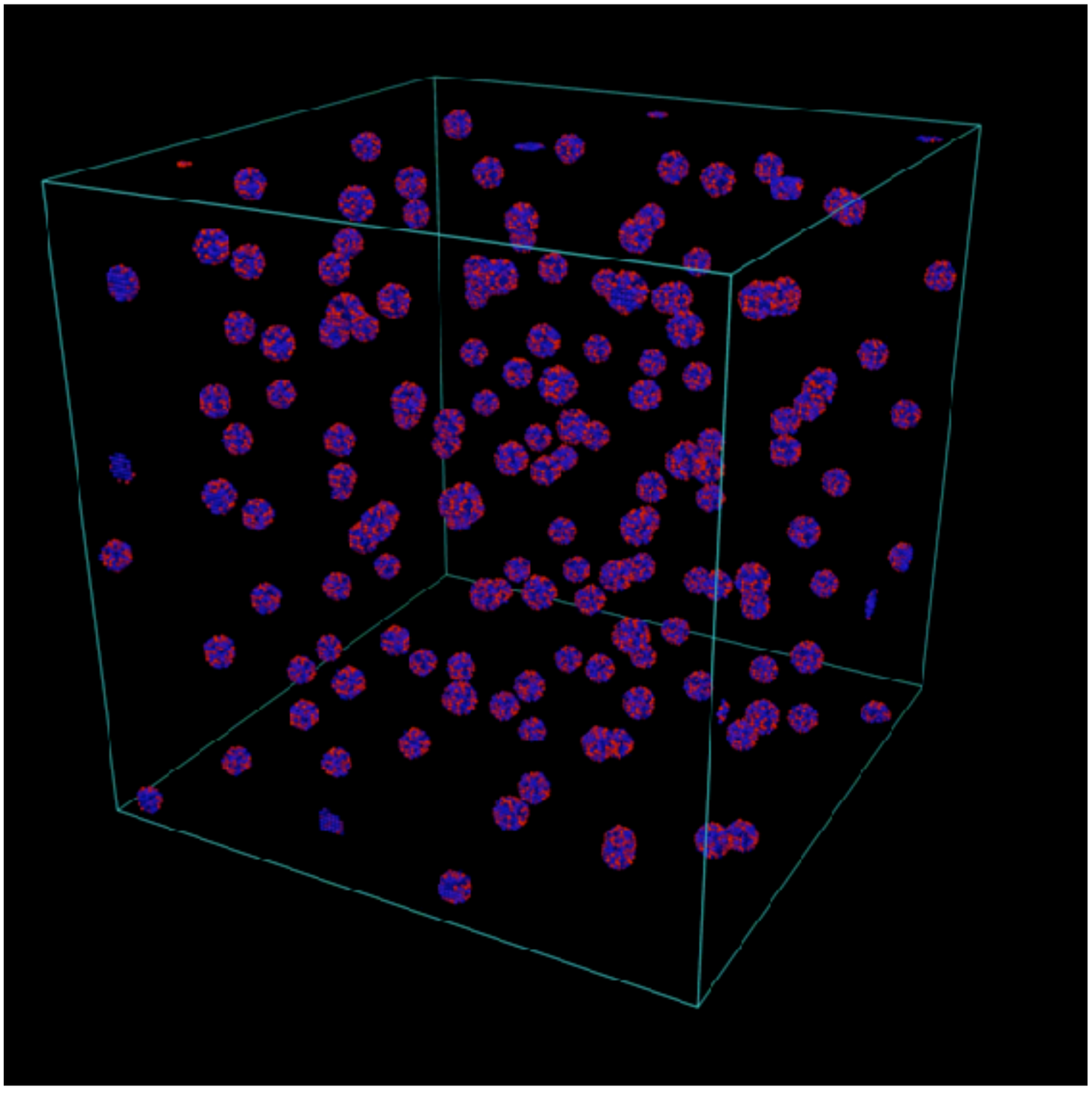

100 keV cascade in Fe(Cr) 10 K

Molecular Dynamics simulation, *mdcask* code

Fe 150x150x150 unit cells -> 6.75 millions atoms

42.8^3 nm^3

pure Cr precipitates 2 nm in diameter

$3x10^{24}$ m^{-3} -> 153 precipitates, 8 nm between them

pka starts at 350 fs

colour depicts kinetic energy (temperature)

green delimits molten volume (E_{kin}>0.16 eV ~ 1'600 °C)

FeCrppt2nm31024_10K100keVrun3

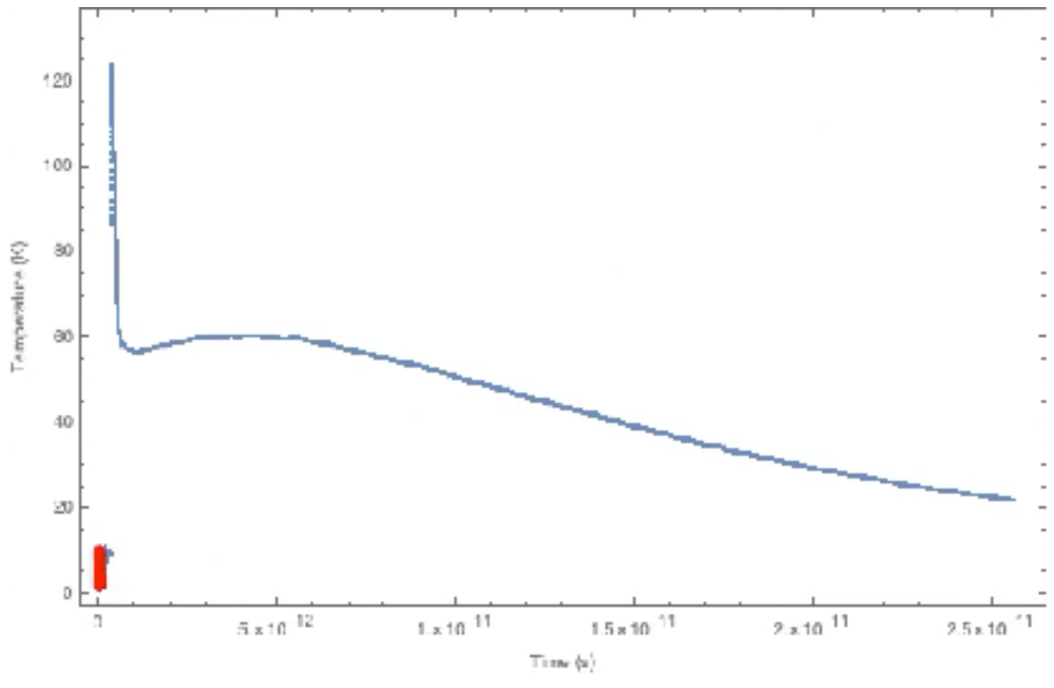

TEM dynamic experiment to see the displacement cascade

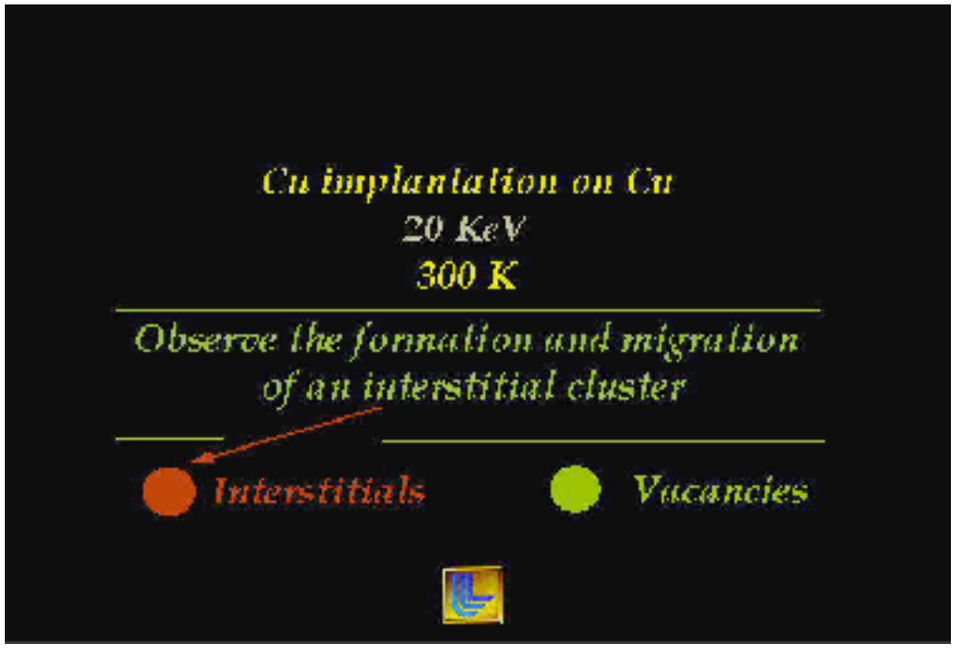

MD simulation, Maria José Caturla

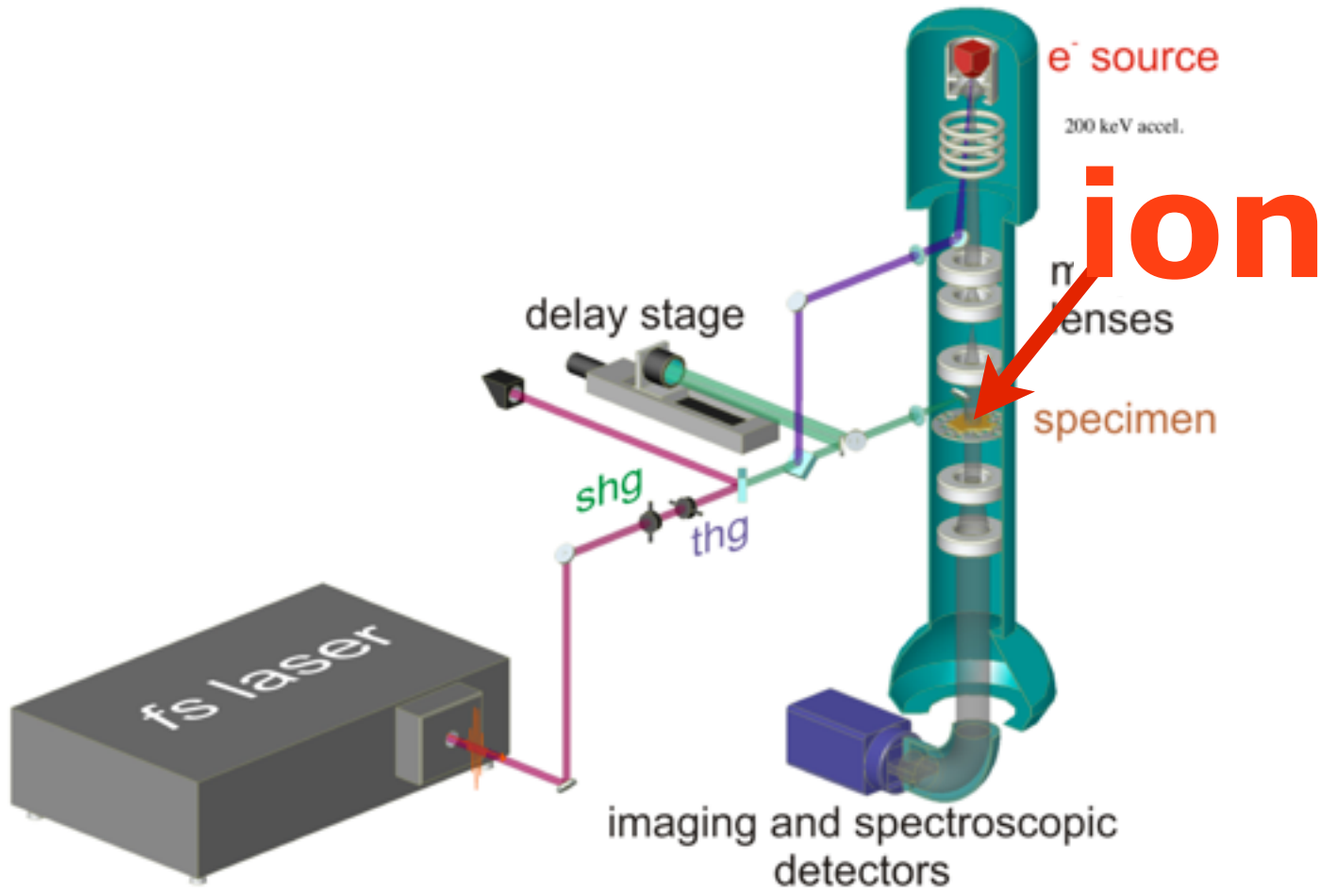

From Brett Barwick, Trinity College, Physics Department, Connecticut, USA

→ **Need for time resolution**. How much?

TEM dynamic experiment : what would we see ?

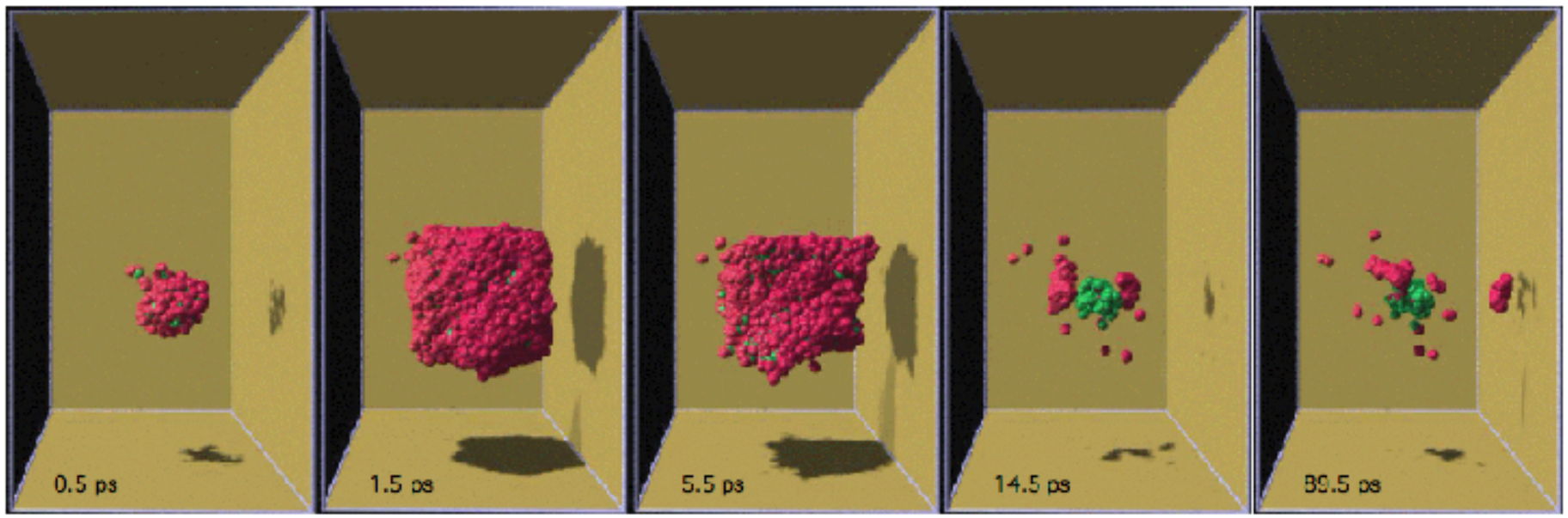

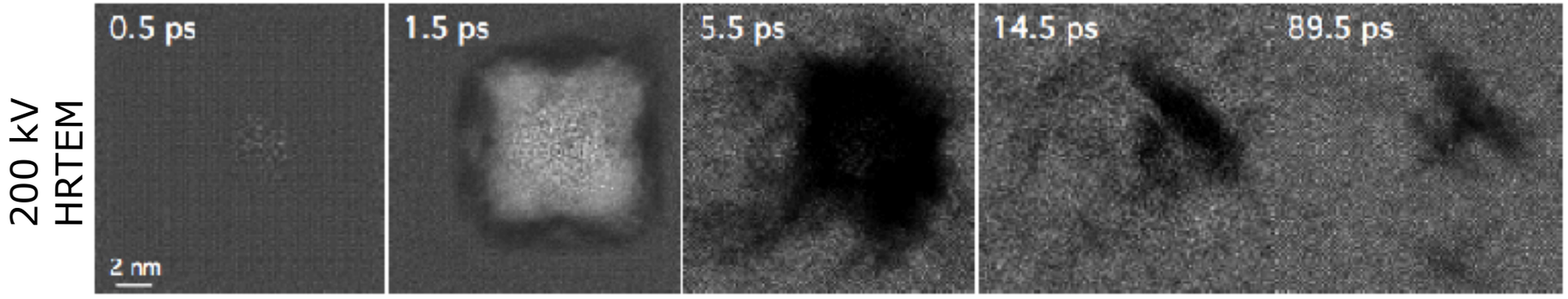

20 keV Cu -> Cu

corresponding simulated TEM images
jEMS software (P. A. Stadelmann)

→ displacement cascade at 1.5 ps makes a 10 nm image; large enough to be easily seen in TEM.

R. E. Schäublin, M.-J. Caturla, M. Wall, T. Felter, M. Fluss, B. D. Wirth, T. Diaz de la Rubia, M. Victoria
Journal of Nuclear Materials, 307-311 (2002) 988-992

TEM contrasts

• Dislocation loops

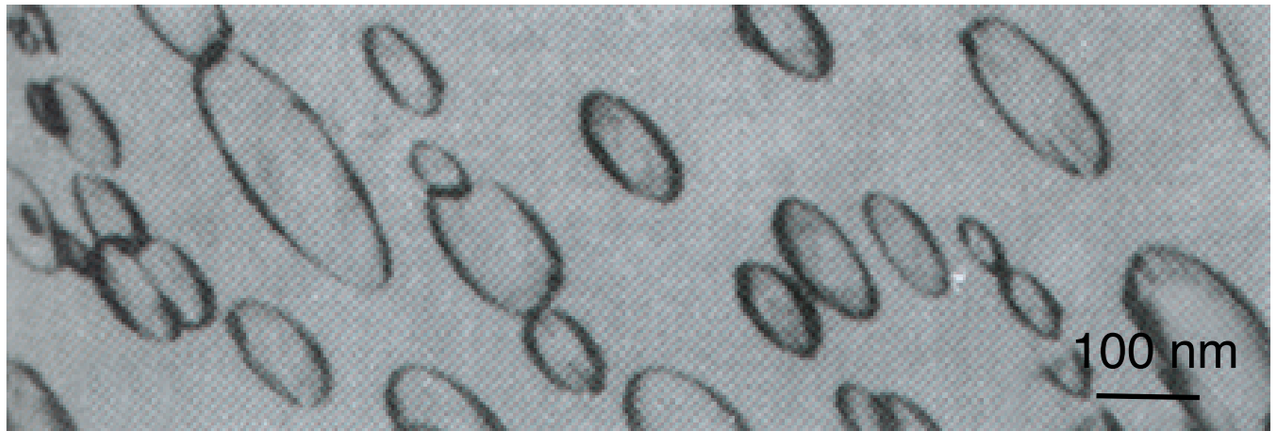

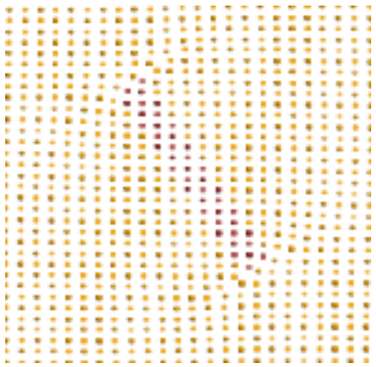

• Cavities voids, gas bubbles

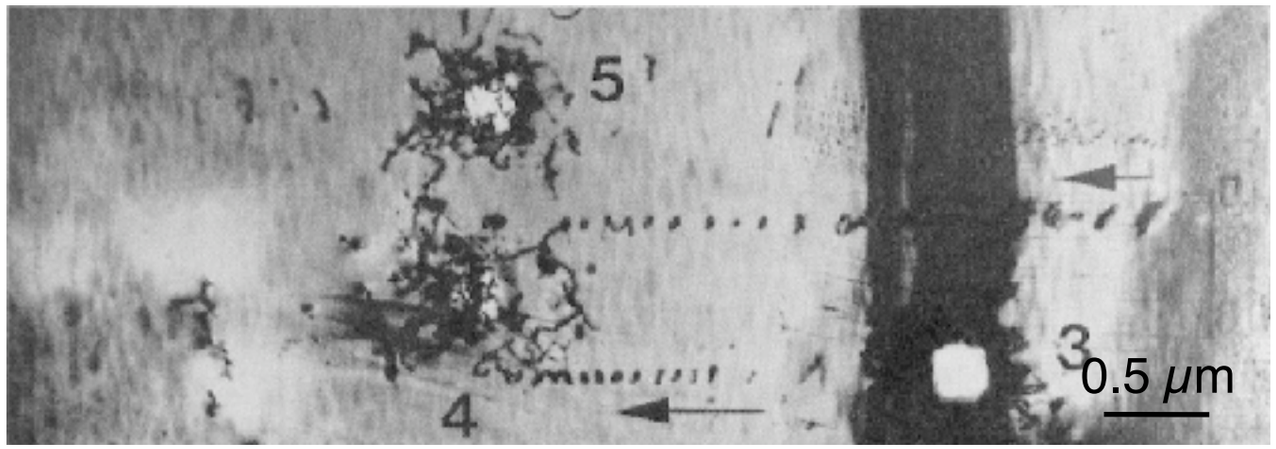

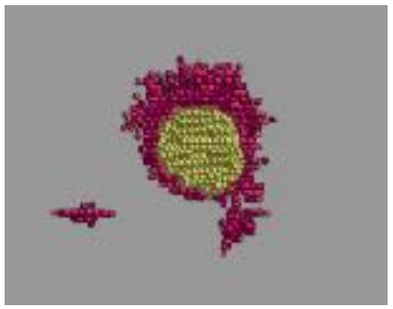

• Stacking fault tetrahedra

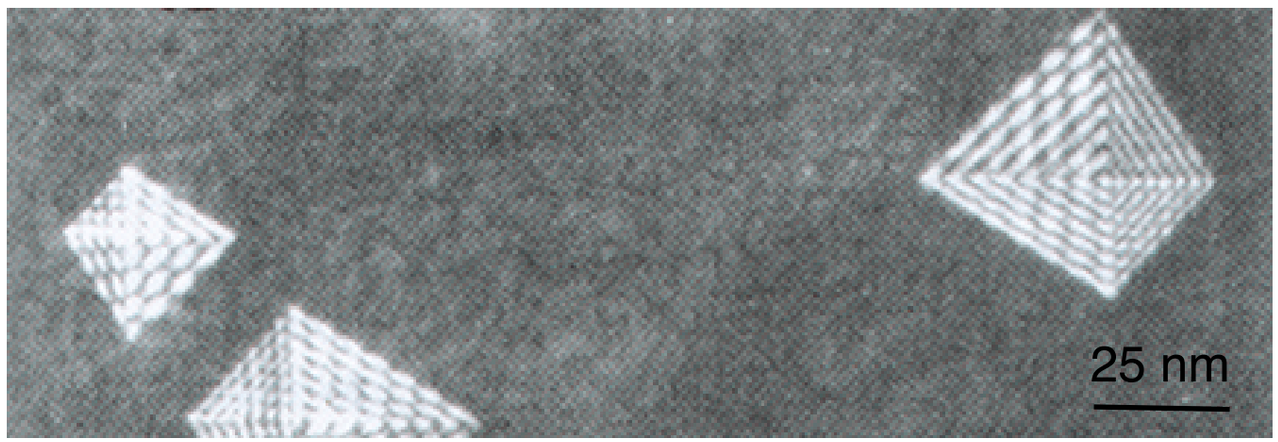

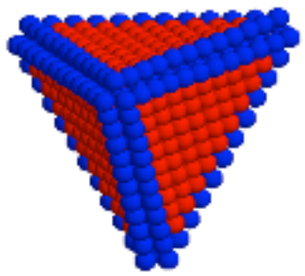

How to relate TEM contrasts to the actual sample features ?

The Utterly Butterly aerobatic team perform at the Zhuhai Airshow 2004 in southern China.

US pair, Melissa Gregory and Denis Petukhov, perform during the Ice Dance 2004 original dance in Nagoya, Japan.

Image interpretation problem ...

Example: stacking fault tetrahedra in irradiated copper

Experiments

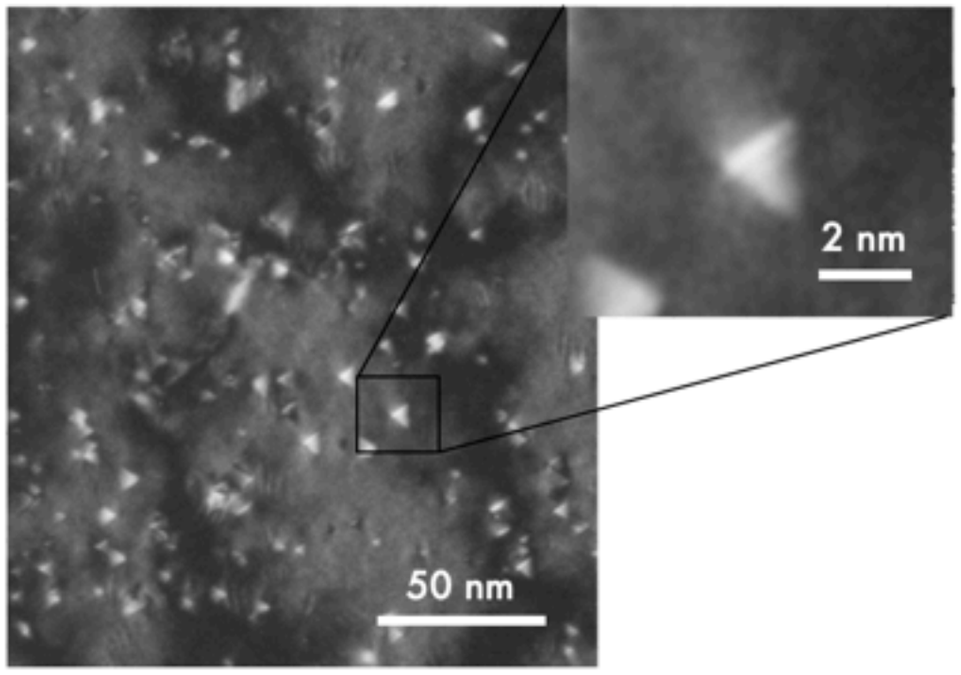

Simulations

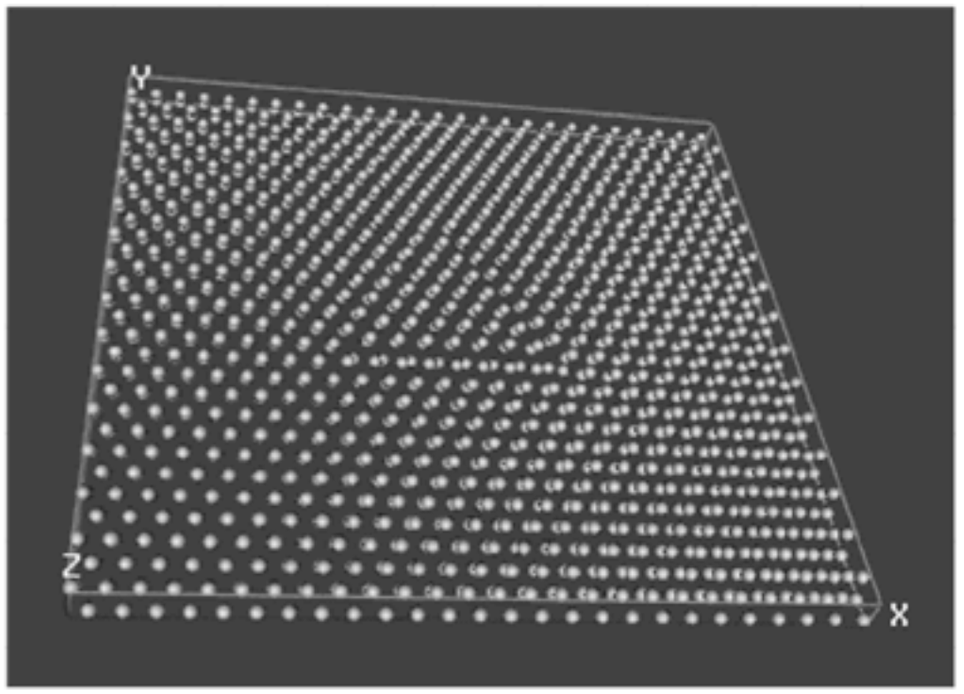

Cu 0.01 dpa RT
weak beam g(6g) g = (200)

Molecular dynamics simulation
Pair potential method, 100’000 atoms

How to close the gap between TEM experimental images and simulations ?

TEM methods

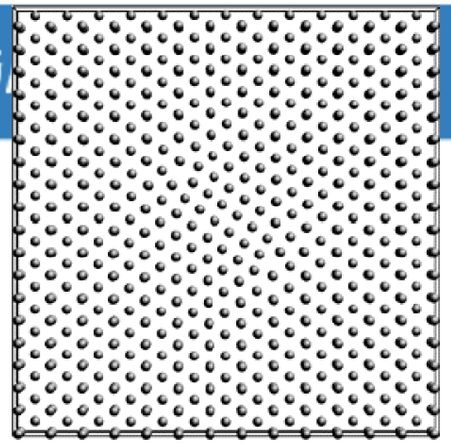

37-interstitial Frank loop in Al

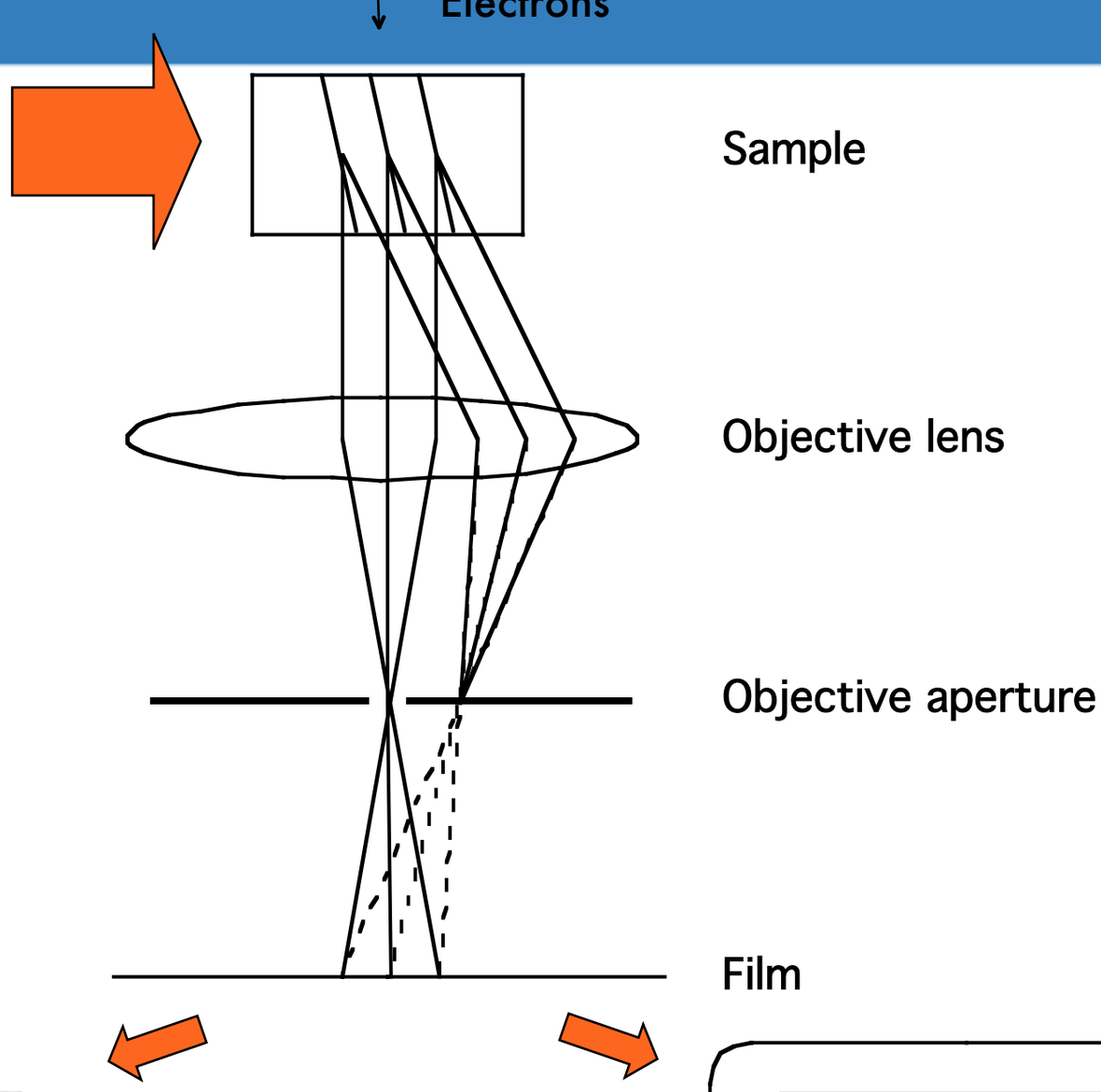

HRTEM

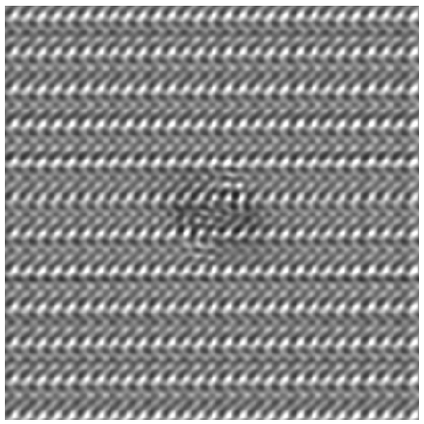

High Resolution imaging mode

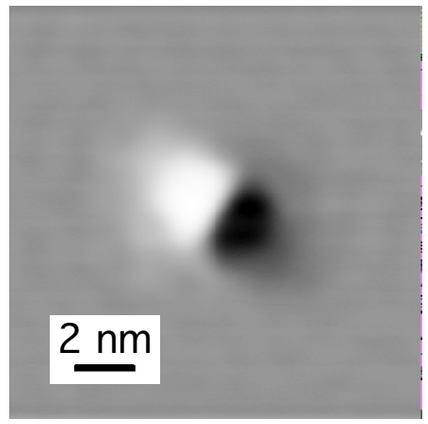

Diffraction contrast imaging mode

CTEM

diffraction limited

TEM image simulations
R. Schäublin

Ewald construction

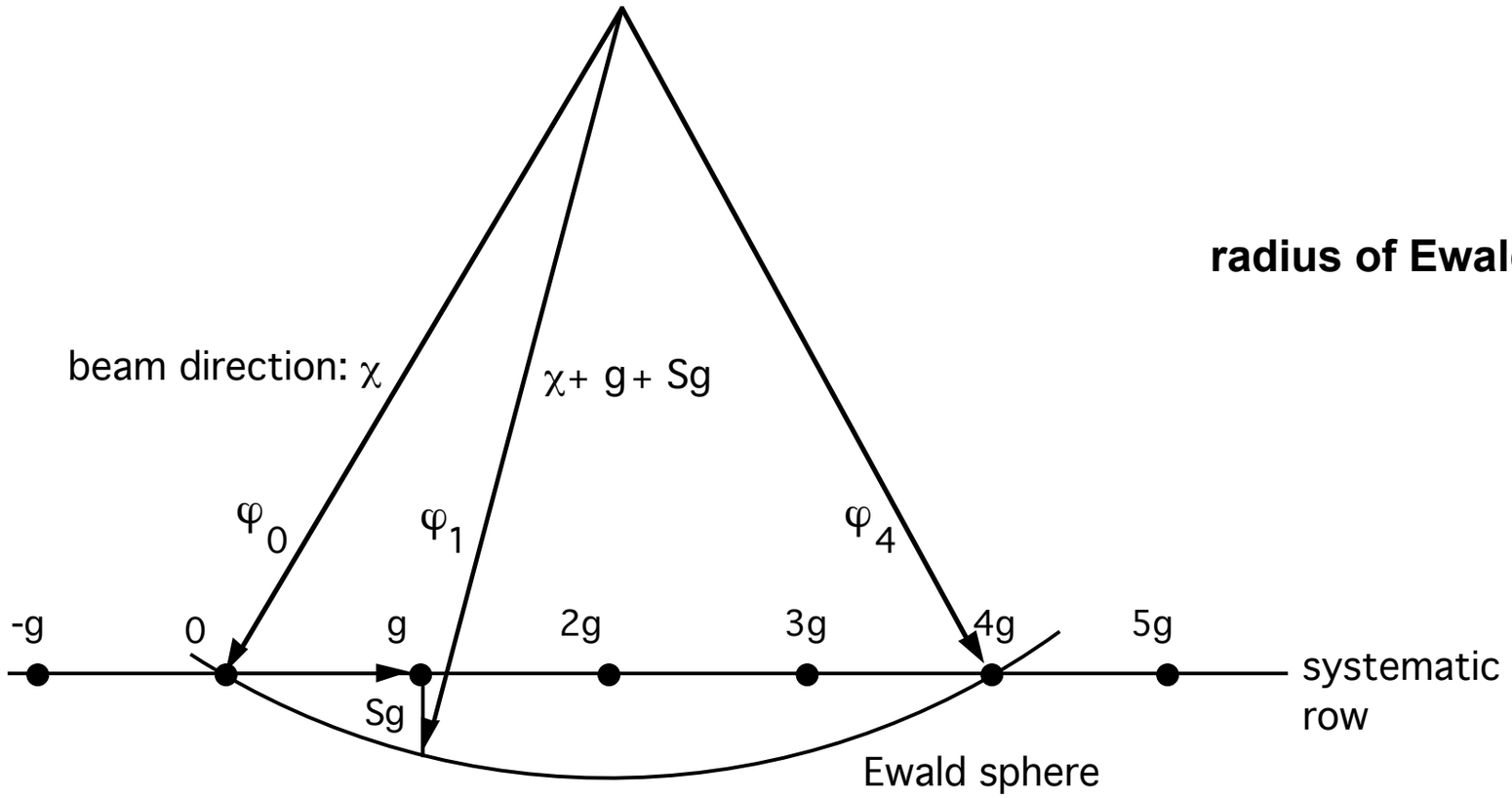

radius of Ewald sphere: 1/λ

Sg: deviation parameter

Crystal and electron beams in reciprocal space in TEM. **χ** is the direction of the transmitted beam, **g** is the reciprocal lattice vector and $\mathbf{s_g}$ the deviation parameter. (**χ** + **g** + $\mathbf{s_g}$) is the direction of diffracted beam with index **g**. **Diffraction condition** quoted as 'm**g**(n**g**)' :

$$s_g = n(n-m)g^2\frac{\lambda}{2}$$

n : excited beam of the systematic row, m : imaging beam
Example: g(4.0g)

Diffraction condition

a• 2-beam dynamical ($s_g = 0$) , bright or dark field

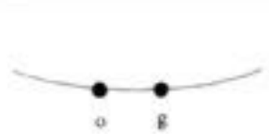

Ewald sphere

DP in microscope

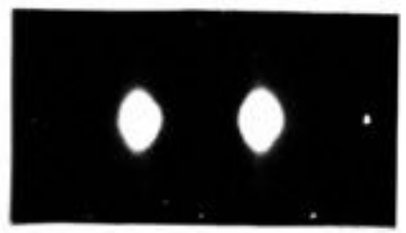

0**g**(1.0**g**) bright field

b• kinematical bright-field ($s_g > 0$)

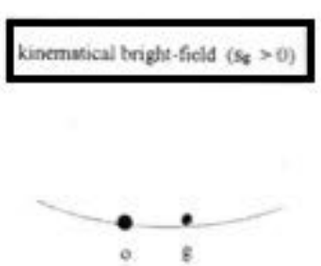

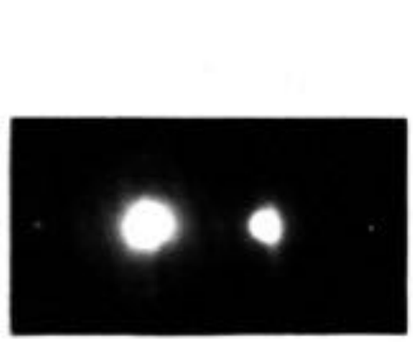

0**g**(1.2**g**) bright field

c• weak-beam ($s_g >> 0$)

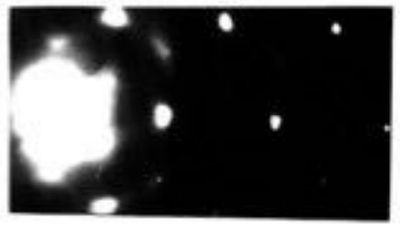

1**g**(3.2**g**) dark field
weak beam

Dislocation in crystal

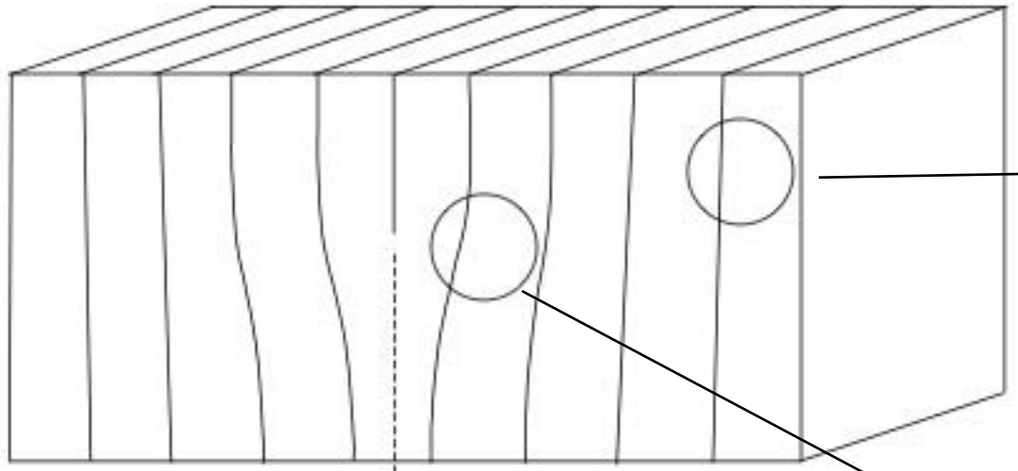

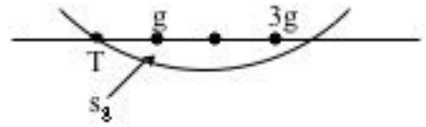

Perfect crystal

Intensity profile

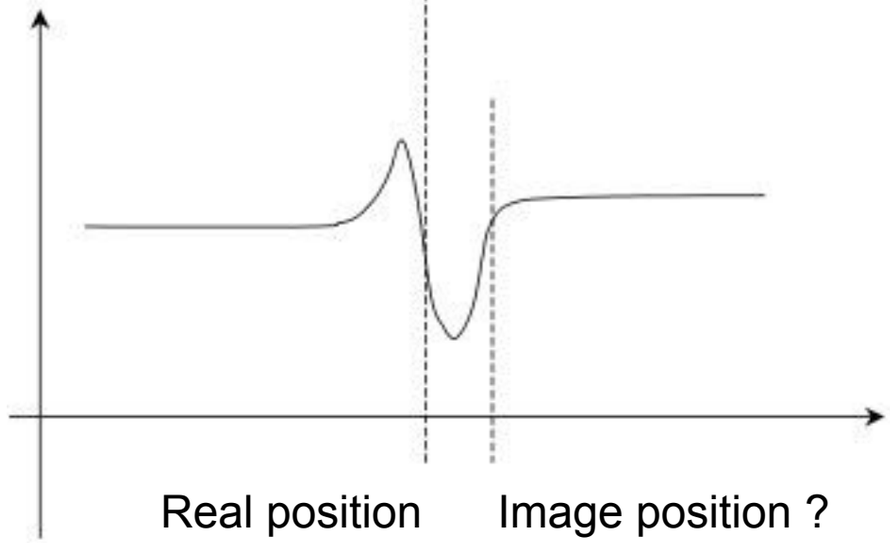

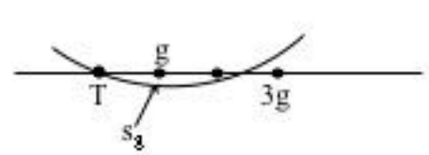

Distorted crystal

Dislocation Burgers vector **b** ? ⇒ **g**·**b** analysis

Dislocation image position ? ⇒ defect sizing, dissociation width, nature

‘g·b analysis’ ➤ Burgers vector

g perpendicular to **b** ➡ dislocation invisible, **g**·**b** = 0

b ➡ 3 unknowns ➡ 3 equations

In practice: minimum 4 different **g**, at least 1 non-coplanar

Edge component give residual contrast
Complete extinction only when **g**·**b** x **u** = 0

Best **g** ? ➡ sharp, thin dislocation contrast

Dislocation density (m^{-2})

Number of intersections N with dislocations made by random straight lines of **length L**
Density = 2 N / L t (**t : foil thickness**)

Problems:
Dislocations lost during sample preparation
Overlapping of dislocations
For a given family of dislocation (same **b**, e.g. in fcc : 1/2<110>) **some are invisible:**

g	Proportion of invisible dislocations
{111}	1/2
{200}	1/3
{220}	1/6
{311}	1/6
{331}	1/6
{420}	all visible

Analysis of dislocation loops

Analysis depends on size d of the loop:

d > 50 nm same as for dislocations

10 nm < d < 50 nm **Inside/outside contrast** analysis (‘coffee bean’ contrast)

d < 10 nm **Black/white contrast** reversal with defect depth

Need for the determination of defect depth and sense of black/white contrast

‘**2 1/2 D technique**’ (Mitchel and Bell 1976)

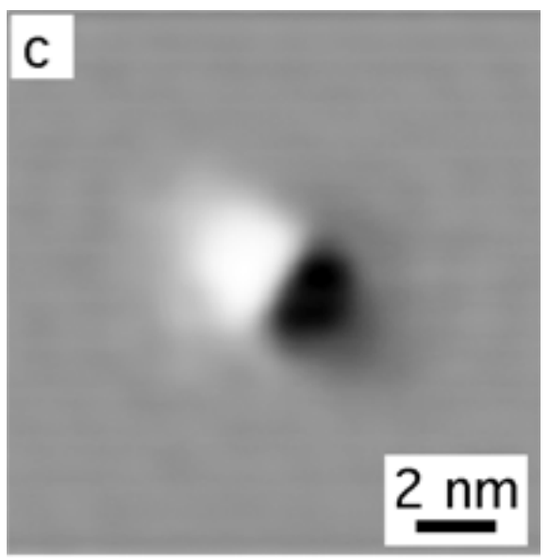

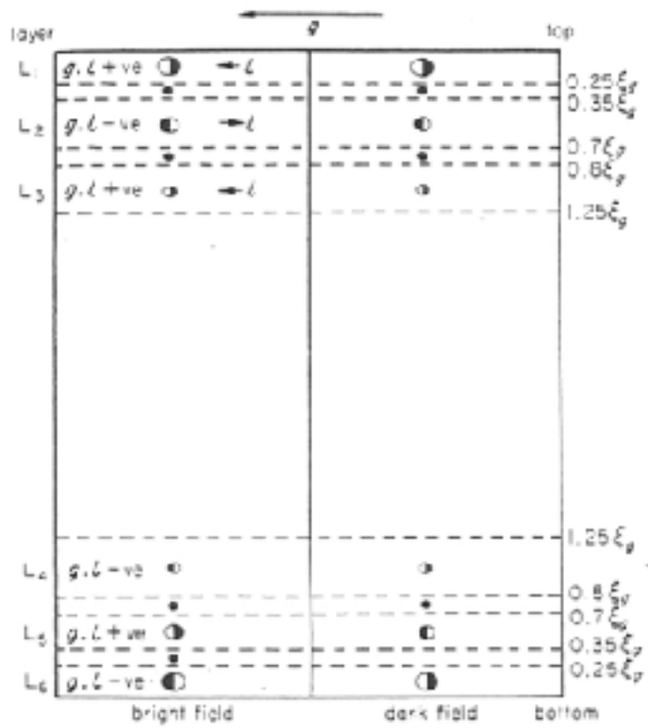

TEM image simulations
R. Schäublin

Nature of dislocation loop: interstitial of vacancy ?

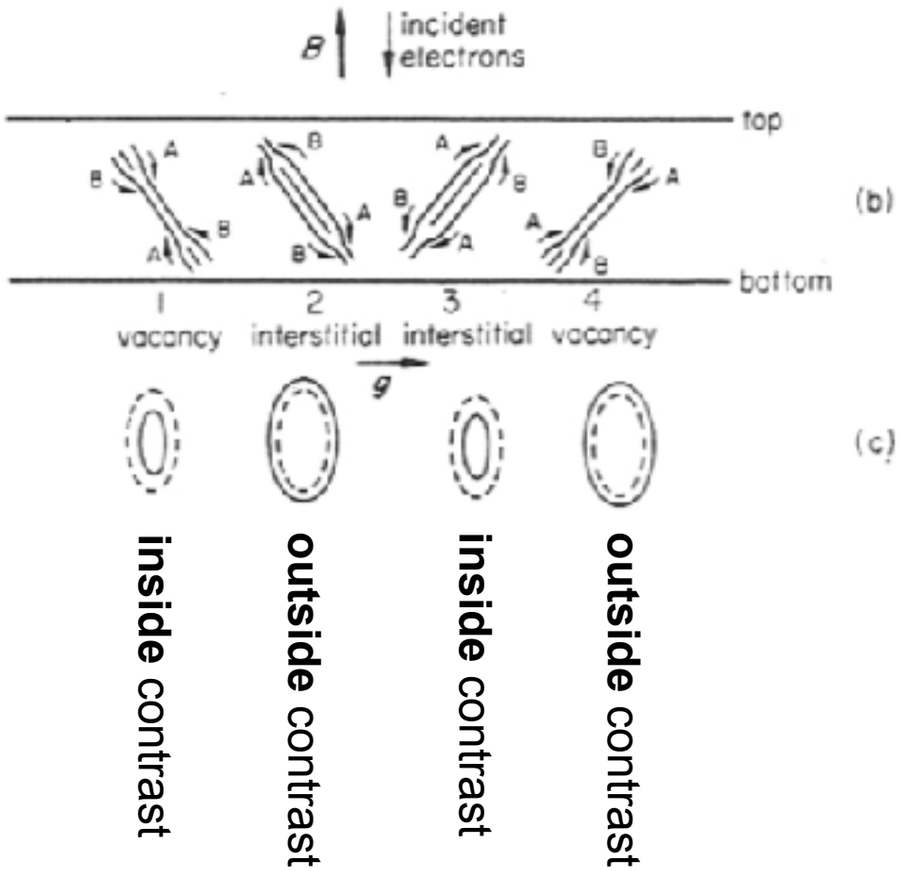

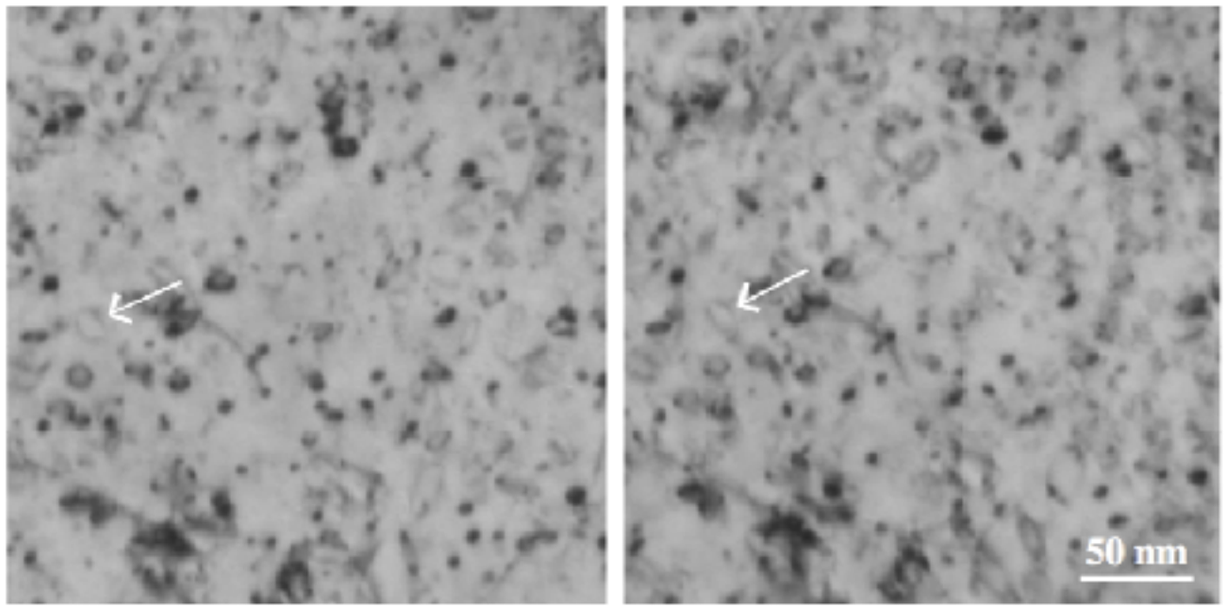

***Figure 1**. Stereo pair of bright field TEM micrograph of F82H irradiated to 8.8 dpa at 302°C with neutrons (irr. # 7) (left and right correspond to eyes). Used for the analysis of the character of loops by the inside-outside contrast method. Arrow points at an outside contrast.*

'inside-outside' contrast analysis needs:

- direction of **g**
- orientation of loop habit plane relative to **g**

Weak beam technique

Extinction distance: $\xi_g = \frac{\pi\Omega\cos\theta}{\lambda f(\theta)}$

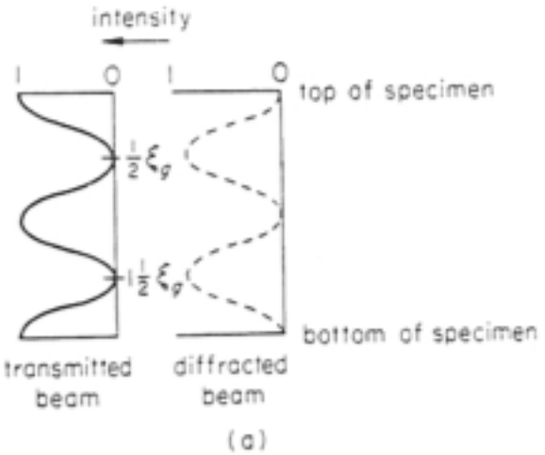

Effective extinction dislocation:

$$\xi_g^{eff} = \frac{\xi_g}{\sqrt{1 + s_g^2 \xi_g^2}}$$

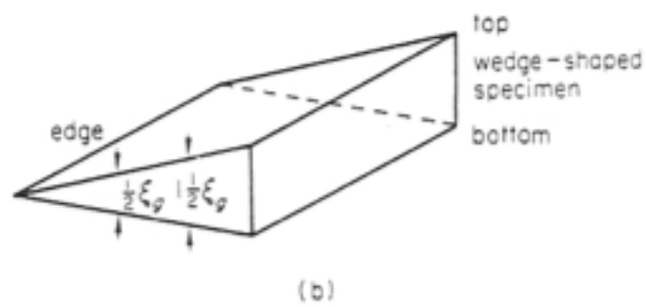

Parameter w: $w = s_g \xi_g$

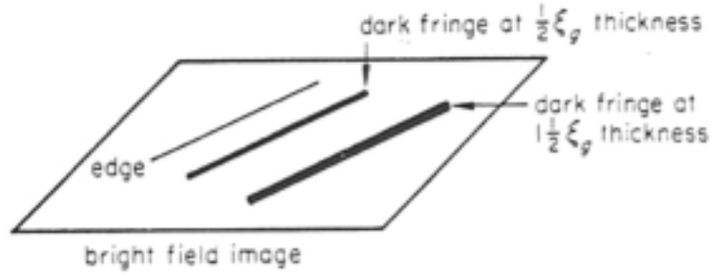

Weak beam technique

(Cockayne, Ray and Whelan 1969)

For copper, 100 kV:
$s_g > 0.2\ nm^{-1}$ ensures a single image per dislocation or partial dislocation

Image position of dislocation is given by: $s_g + \frac{d}{dz}(gR) = 0$
The “turning point”

Dislocation contrast width: $\frac{\xi_g^{eff}}{3}$

TEM image simulation

TEM image simulation

Every image detail, or contrast, appearing on the phosphorescent screen of a transmission electron microscope (TEM) is the result of the interaction of the electron beam with the sample. Unlike the direct interpretation we can give of the eye visible world, the interpretation of TEM micrographs is far from straightforward and has to be considered carefully. The origins of the TEM contrasts are complex and multiple. They are divided here into the following four categories:

Absorption contrast,
Diffraction contrast,
Phase contrast.

The contrast formation theories, even though based on sometimes tricky approximations, give a good description of the TEM images. With the help of these theories, the TEM images can be reproduced by large numerical calculations. The image simulation appears as a powerful tool for the identification of an object at the origin of an observed contrast.

TEM image simulation

There are two main types of simulation techniques:

1) **Many beam calculation**
2) **Multislice calculation**

The **many beam calculation** originates from the calculation of intensities of X-Ray diffraction (1930's). The idea is to integrate the various beams seen in diffraction along a thin column going trough the specimen. At the end of the integration one gets the intensity of the pixel beneath the column. In TEM it is well known for the case of two beams, the transmitted and one diffracted beam. They form the equations of Howie and Whelan. While they work fine for most of the cases in CTEM, i.e. imaging performed in bright field and dark field, where 90 % of the intensity in concentrated in these two beams, it does not hold true anymore for dark field weak beam (or in kinematical condition), which is needed for higher contrast and higher spatial resolution. Thus the need for many beam calculation.
It takes into account:
1) the displacement field of the defect configuration and
2) the diffraction condition.

The **multislice technique** originates from the first calculations of high resolution atomic images of perfect crystal structures by Cowley and Moodie (1957). The idea is to propagate an incident planar electron wave through thin slices composing the specimen, slice after slice.
It takes into account:
1) the atomic positions in the sample.

Many beam calculation

Many beam calculation

A summary of the theory of electron propagation in thin crystals is given here, as it will help to understand beam contribution in the many beam calculation. To calculate the propagation of electrons in a faulted crystal, we use the dynamical theory of contrast (see Hirsch et al. [Hirsch, 1969]). The crystal at a point r is described by a faulted potential V(r) that can be written as a Fourier serie:

$$V(r) = \frac{h^2}{2\, m_e} \sum_g \left[U_g \exp\left(-2\pi i\, gR(r)\right) \right] \exp\left(2\pi i\, gr\right)$$

The summation is done over all reciprocal lattice vectors g, with m_e the electron mass and h the Planck constant. R(r) describes the displacement field around the lattice defect. The Schrödinger's wave equation is:

$$\nabla^2\psi(r) + \left(\frac{8\pi^2 m_e}{h^2}\right)\left[E + V(r)\right]\psi(r) = 0$$

ψ(r) is the function associated to the electron wave that moves through the faulted crystal. The proposed solution to the Schrödinger equation is:

$$\psi(r) = \sum_g \varphi_g \exp\left(2\pi i\,(\chi + g + s_g)r\right)$$

The $\phi_g(r)$ function are associated with the beams that come out of the sample, including the transmitted beam (beam 0) and the diffracted beams (beam 1 to n). The contrast intensity I recorded on the micrographs for a g image, is simply $I=\phi_g(r)\cdot\ \overline{\phi}_g(r)$.

Many beam calculation

We will take a co-ordinate η_g along every beam direction. We then substitute V(r) and ψ(r) in the Schrödinger equation. We obtain a system of n differential equations of the first order with n unknowns $\phi_g(r)$:

$$\frac{\partial \varphi_g(r)}{\partial \eta_g} \cong \sum_h \frac{\pi i}{\xi_{g-h}} \varphi_h(r) \exp\left(2\pi i (h-g)R(r) + 2\pi i (s_h - s_g)r\right)$$

The equations are to be integrated along the proper beam direction η_g. This is difficult to solve analytically. To simplify, we use the column approximation that allows to make the integration along the same direction for all beams.

- **Column approximation**: $\frac{\partial}{\partial \eta_g} \cong \frac{d}{dz}$

The column approximation means that we consider only the direction of the transmitted beam to make the integration.

Many beam calculation

We can then write the **equation system** in a **matrix form**:

$$\frac{d\phi(r)}{dz} = M\,\phi(r) \quad \text{where:} \quad \phi(r) = \begin{bmatrix} \varphi_0 \\ \varphi_1 \\ \vdots \\ \varphi_n \end{bmatrix}$$

The matrix M is symmetrical and has the following expression: (also called **scattering matrix**)

$$\begin{vmatrix} A & A_1 & \dots & A_i & \dots & A_n \\ A_1 & B_1 & & & & \\ & & & & C_{ij} & \\ A_i & & & B_i & & \\ & & C_{ij} & & & \\ A_n & & & & & B_n \end{vmatrix}$$

Many beam calculation

Where the coefficients are:

$$A = -\frac{\xi_1}{\xi'_0}$$

$$A_i = i\xi_1\left(\frac{1}{\xi_i} + \frac{i}{\xi'_i}\right)$$

$$B_i = \left[-\frac{\xi_1}{\xi'_0} + 2i s_i \xi_1 + 2\pi i \frac{d}{dz}(g_i R(r))\right]$$

$$C_{ij} = i\xi_1\left(\frac{1}{\xi_{i-j}} + \frac{i}{\xi'_{i-j}}\right)$$

ξ_i is the **extinction distance** which becomes large if the beam i gets far from the transmitted beam; ξ'_i is proportional to ξ_i. ξ_1 is a scaling factor that was originally introduced by Head et al. to avoid convergence problems and save calculation time in the integrations.

We can then compute $d\phi_0(r)/dz$:

$$\frac{d\varphi_0}{dz} = -\frac{\xi_1}{\xi_0'}\varphi_0 + \cdots + i\xi_1\left(\frac{1}{\xi_i} + \frac{i}{\xi_i'}\right)\varphi_i + \cdots + i\xi_1\left(\frac{1}{\xi_n} + \frac{i}{\xi_n'}\right)\varphi_n$$

The general equation for a $d\phi_i(r)/dz$ is:

$$\frac{d\varphi_k}{dz} = i\xi_1\left(\frac{1}{\xi_i} + \frac{i}{\xi_i'}\right)\varphi_0 + \cdots + i\xi_1\left(\frac{1}{\xi_{i-j}} + \frac{i}{\xi_{i-j}'}\right)\varphi_j + \cdots$$

$$\cdots + \left(-\frac{\xi_1}{\xi_0'} + 2i\,s_i\xi_1 + 2\pi i\,\frac{d}{dz}(g_i\,R(r))\right)\varphi_i + \cdots + i\xi_1\left(\frac{1}{\xi_{i-n}} + \frac{i}{\xi_{i-n}'}\right)\varphi_n$$

These equations show that the derivative of each beam is a linear combination of all the beams. The contribution of each beam in the linear combination is weighted by the matrix coefficients.

The physical meaning of these relations is that the contribution of a beam i depends on the associated deviation parameter s_i (diffraction condition), the associated extinction distance ξ_i (material characteristics) and a cross-term ξ_{i-j} that has the expression of an extinction distance.

High |i| values correspond to large ξ_i and therefore beam i may have a weak contribution; but when this same beam has a small deviation parameter s_i, it may have a strong contribution. It appears that the importance of a beam (i) contribution is a balance between s_i, deduced from the observation conditions and ξ_i, given by the material characteristics. This had to be taken into account in the choice of the beams included in the calculation.

General rule to choose beams for calculation: **(1) beams have to be close to the transmitted beam** (**small ξ_i**) and **(2) close to the Ewald sphere** intersections with the systematic row (**small s_i**).

Many beam calculation

Data required to make an image simulation:

Material:
- Space group,
- Lattice parameter,
- Atomic positions,
- Elastic constants (unit:10^{12} dyne/cm^2)

Geometry (based on the Head et al. program, dimension unit: nm):
- Foil normal,
- Electron beam direction,
- Dislocation line direction,
- Burgers vector for each dislocation, set to 1/1[0,0,0] if no dislocation,
- Fault plane normal (plane related by adjacent dislocations), set to [0,0,0] if no plane,
- Lattice translation vector (in the above mentioned plane), set to 1/1[0,0,0] if no fault on plane,
- Width of plane,
- Thickness of the thin foil.

Diffraction condition:
- Acceleration voltage,
- When you have a weak beam condition (e.g. g=[002], g(4g)) the diffraction condition is described by:
  - One diffraction vector (g=[002]),
  - The vector describing the projection of the Ewald sphere center on the systematic row (2g=[004]),
  - (centre of the Laue circle)
- If you have additional diffraction spots (out of the systematic row), describe them as follows:
  - Diffraction vector,
  - Deviation parameter.

Many beam calculation

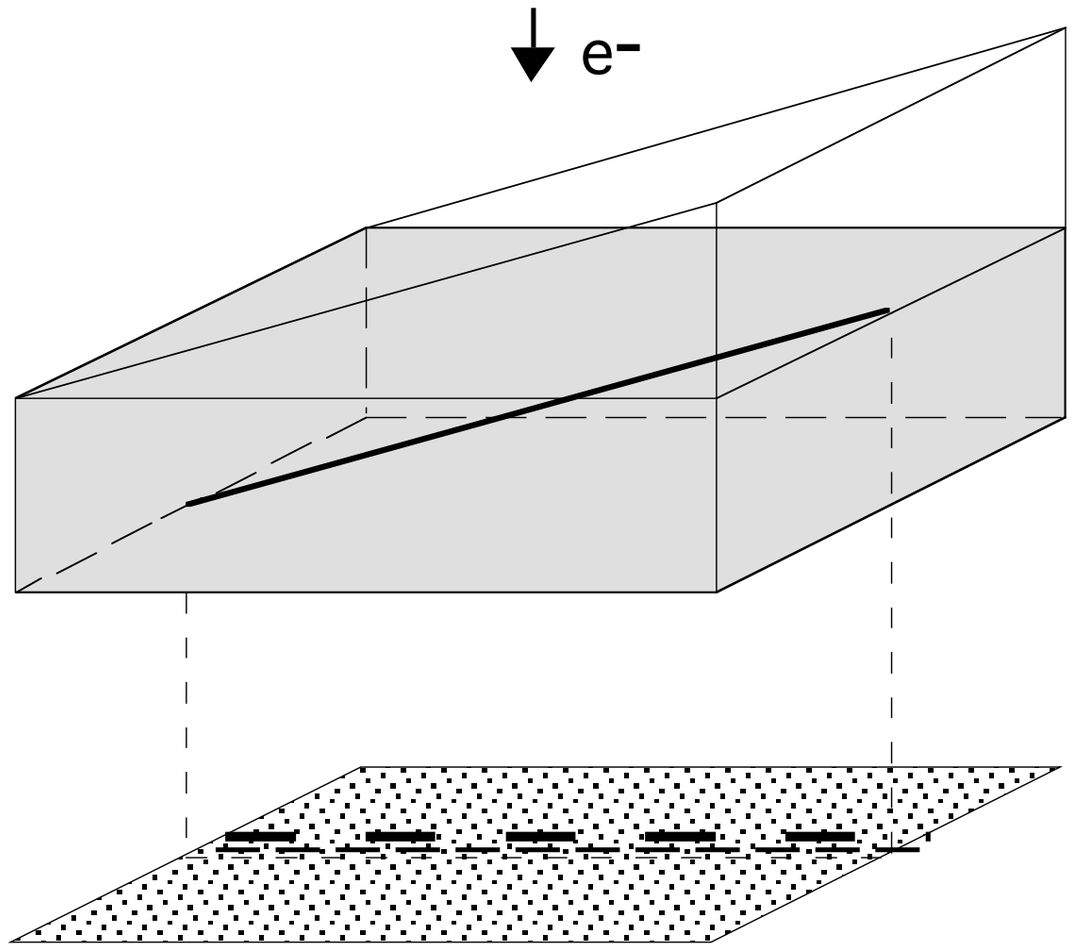

"Generalised cross-section"

thin foil with one dislocation

image

Many beam calculation : example

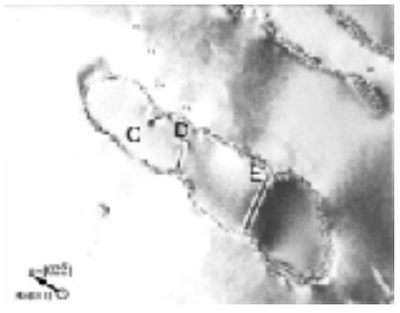

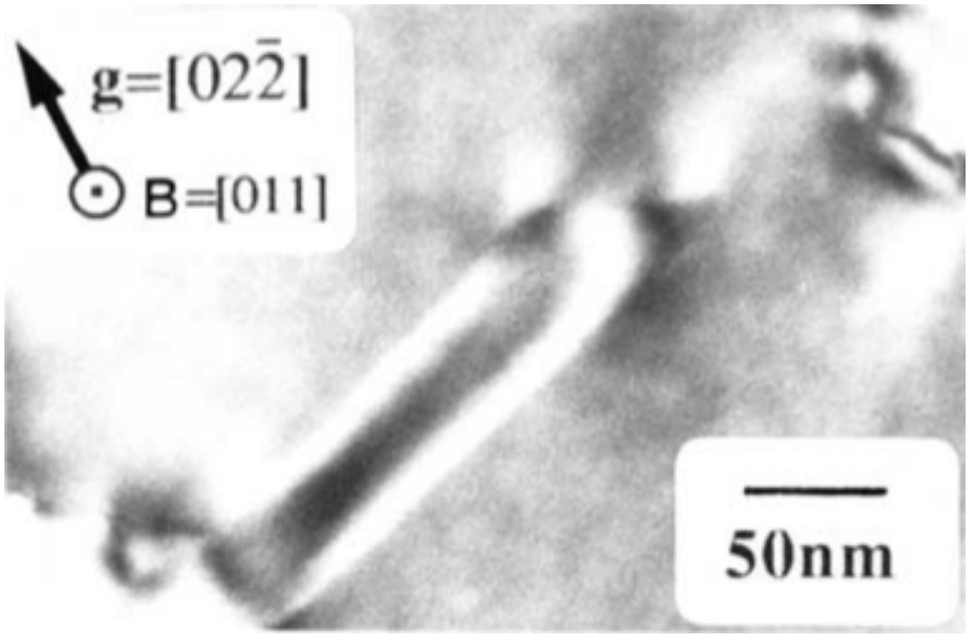

Experiment

CUFOUR software

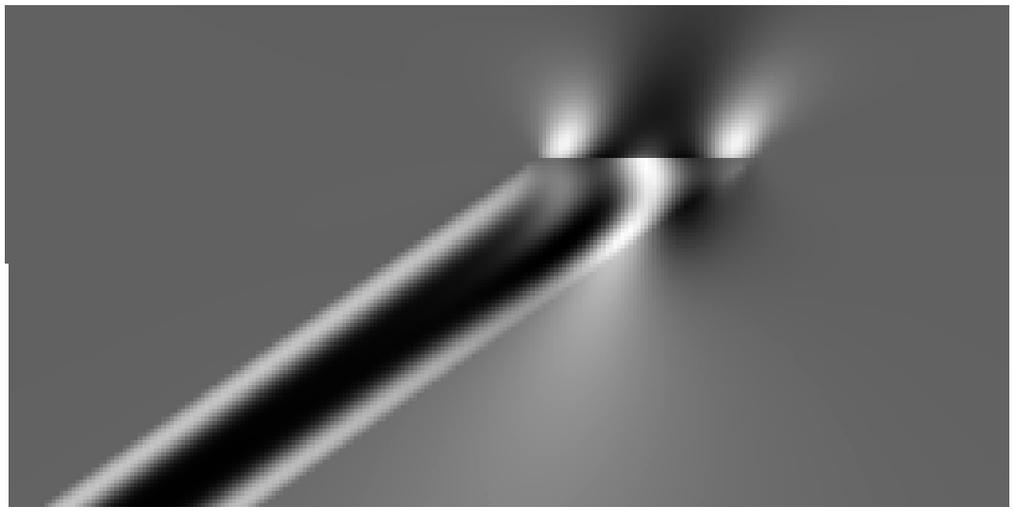

Simulation

Simulated TEM image of α-fringes bordered by a 1/2 [-1 -1 0] dislocation in γ' precipitate of a $Ni_3(Al,Ta)$ superalloy.

- Matching to TEM experimental image ➤ **lattice translation = ~1/10 [0 1 0] ~ 20 pm precision**
- **Attributed to Ni segregation**

What about the column approximation ?

Non-column approximation formulation:

Theory: the Howie-Basinski equations

Imperfect crystal $V(\mathbf{r}) = \sum_g V_g e^{2\pi i \mathbf{g}\cdot(\mathbf{r}-\mathbf{R}(\mathbf{r}))}$ + **Bloch wave theorem** $\psi(\mathbf{r}) = \sum_g \left[\phi_{\mathbf{g}}(\mathbf{r}) e^{2\pi i(\mathbf{k}+\mathbf{g}+\mathbf{s_g})\cdot\mathbf{r}}\right]$

$$-\frac{\hbar^2}{2m}\nabla^2\psi(\mathbf{r}) + V(\mathbf{r})\psi(\mathbf{r}) = E\psi(\mathbf{r})$$

$$(\mathbf{k}+\mathbf{g}+\mathbf{s_g})_x\frac{\partial\Phi_g}{\partial x} + (\mathbf{k}+\mathbf{g}+\mathbf{s_g})_y\frac{\partial\Phi_g}{\partial y} + (\mathbf{k}+\mathbf{g}+\mathbf{s_g})_z\frac{\partial\Phi_g}{\partial z}$$
$$= -\sum_{g'}(1-\delta_{gg'})\pi i U_{g-g'}\Phi_{g'} + 2\pi i(\mathbf{k}+\mathbf{g}+\mathbf{s_g})_z s_{g\_R}\Phi_g$$

- Non-column approximation is possible but more complex to integrate numerically

CUFOUR → **CuView** software at http://scopem-cuview.ethz.ch:8080

Multislice calculation

Multislice technique

$\Psi(r)_j = [\Psi(r)_{j-1} \bullet q_j] \times p_{j->j+1}$
$\Psi(r)_j$: Wave function entering slice j+1,
q_j : Function of the transmittance of the slice j,
$p_{j->j+1}$: Function of propagation (propagator) from slice j to slice j+1.

Reference:
J.M. Cowley, A.F. Moodie,
Acta Cryst. 10 (1957) 609.

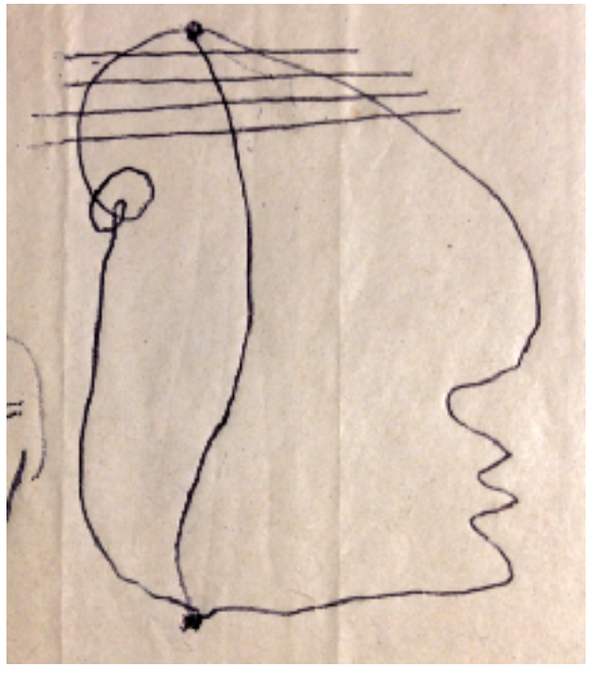

A.F. Moodie, Cambridge, summer 1995

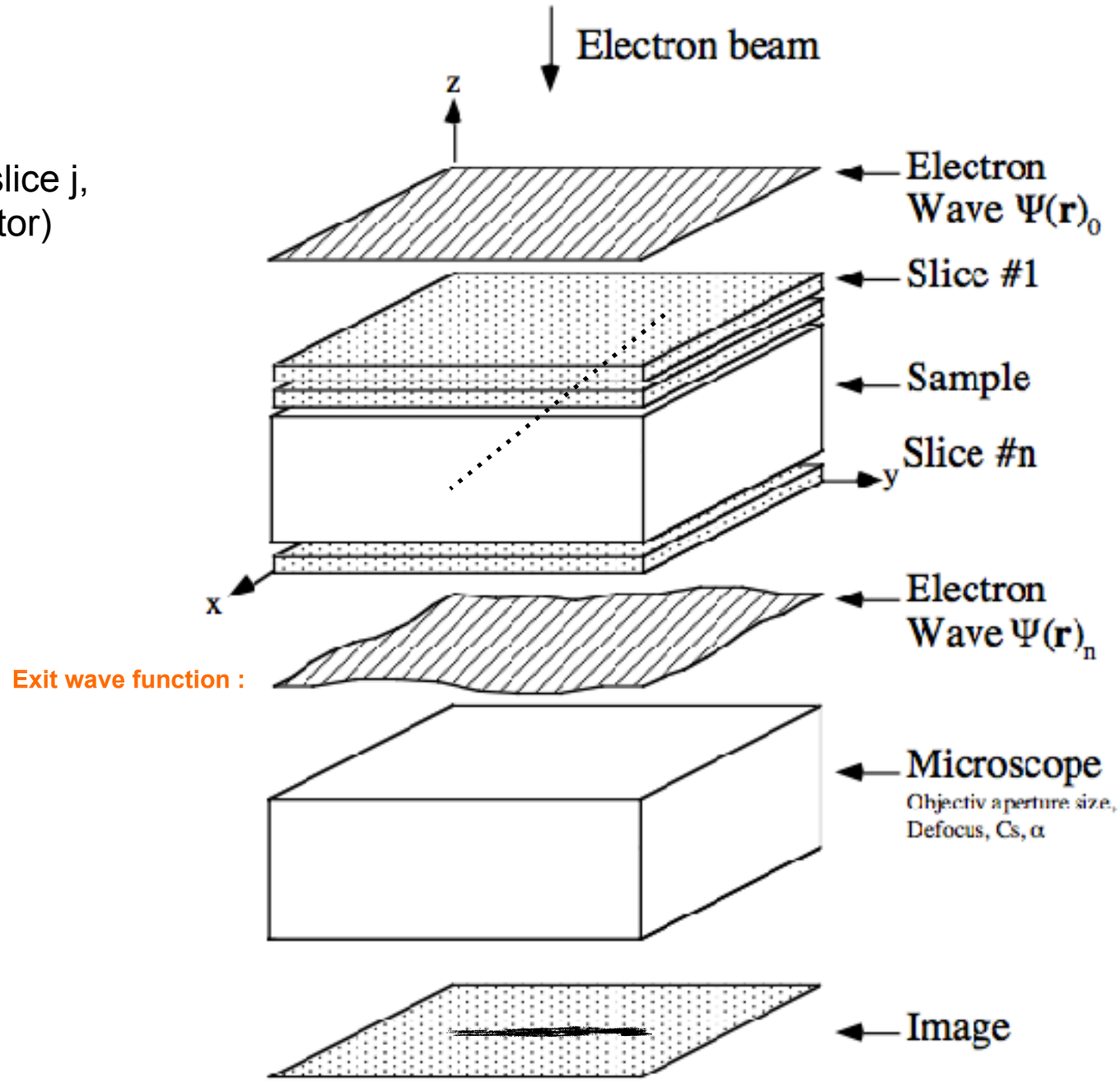

Exit wave function :

Multislice technique

Data required to make an image simulation:

Material:

Atomic positions (no limit in the number of atoms !)

Diffraction condition:

Acceleration voltage

That is all !

HR-TEM image of a precipitate in Mg(Zn,Ca)

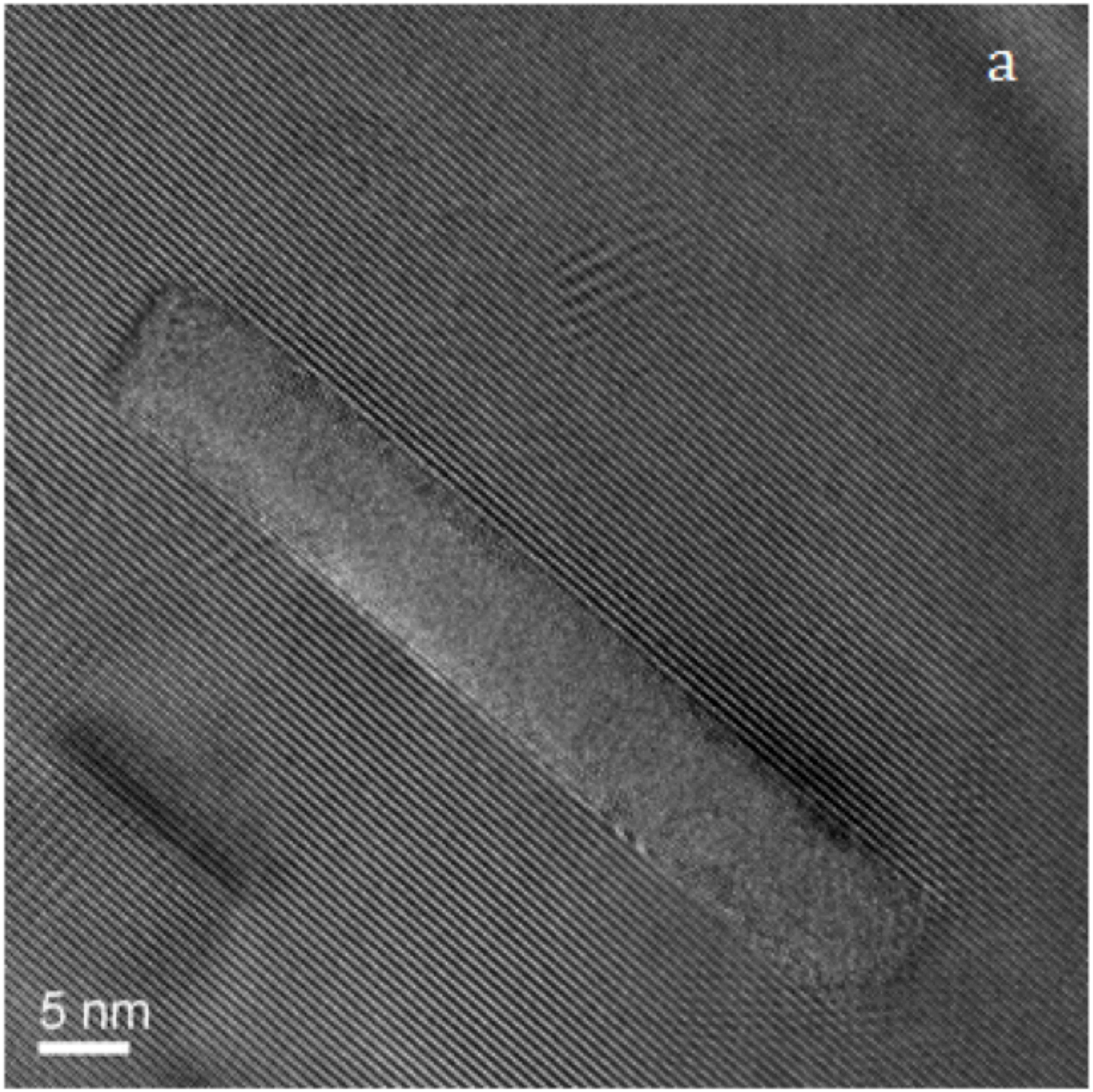

Example of HR-TEM image simulation of a perfect crystal of fiotite

Unit cell:

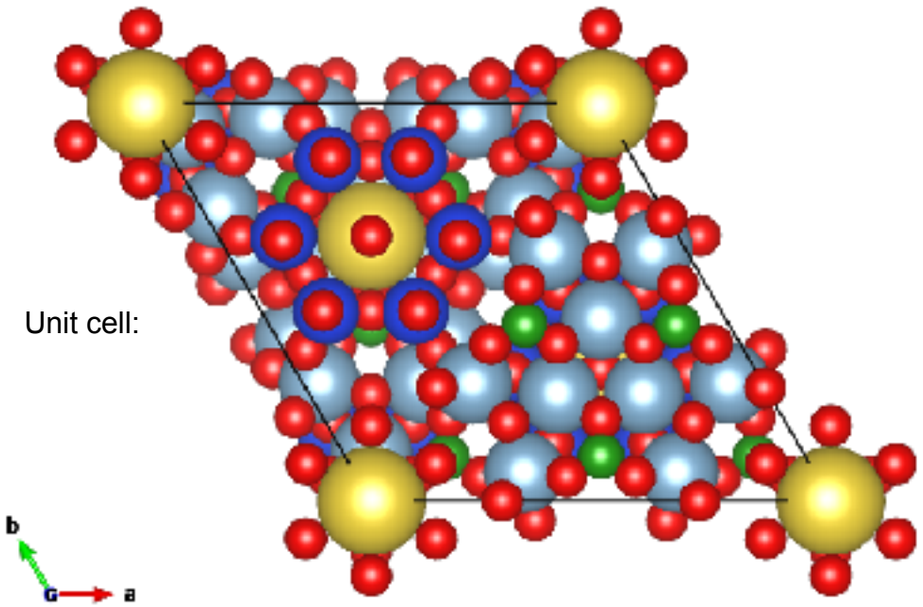

3x3 unit cells:

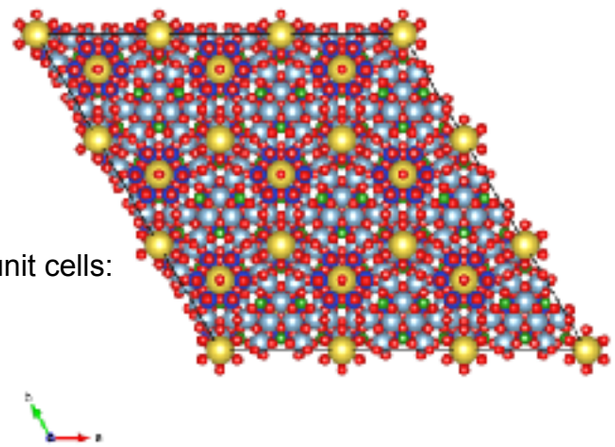

```
Crystal system: trigonal
Space group name    R 3 m (Hermann-Mauguin symbol)
Space group number  160
Lattice parameters (nm, degree):
   a        b        c       alpha    beta     gamma
15.96700 15.96700  7.12600  90.0000  90.0000 120.0000
204 atoms: Na, Al, Fe, Mn, Mg, Li, Si, O
```

phase contrast

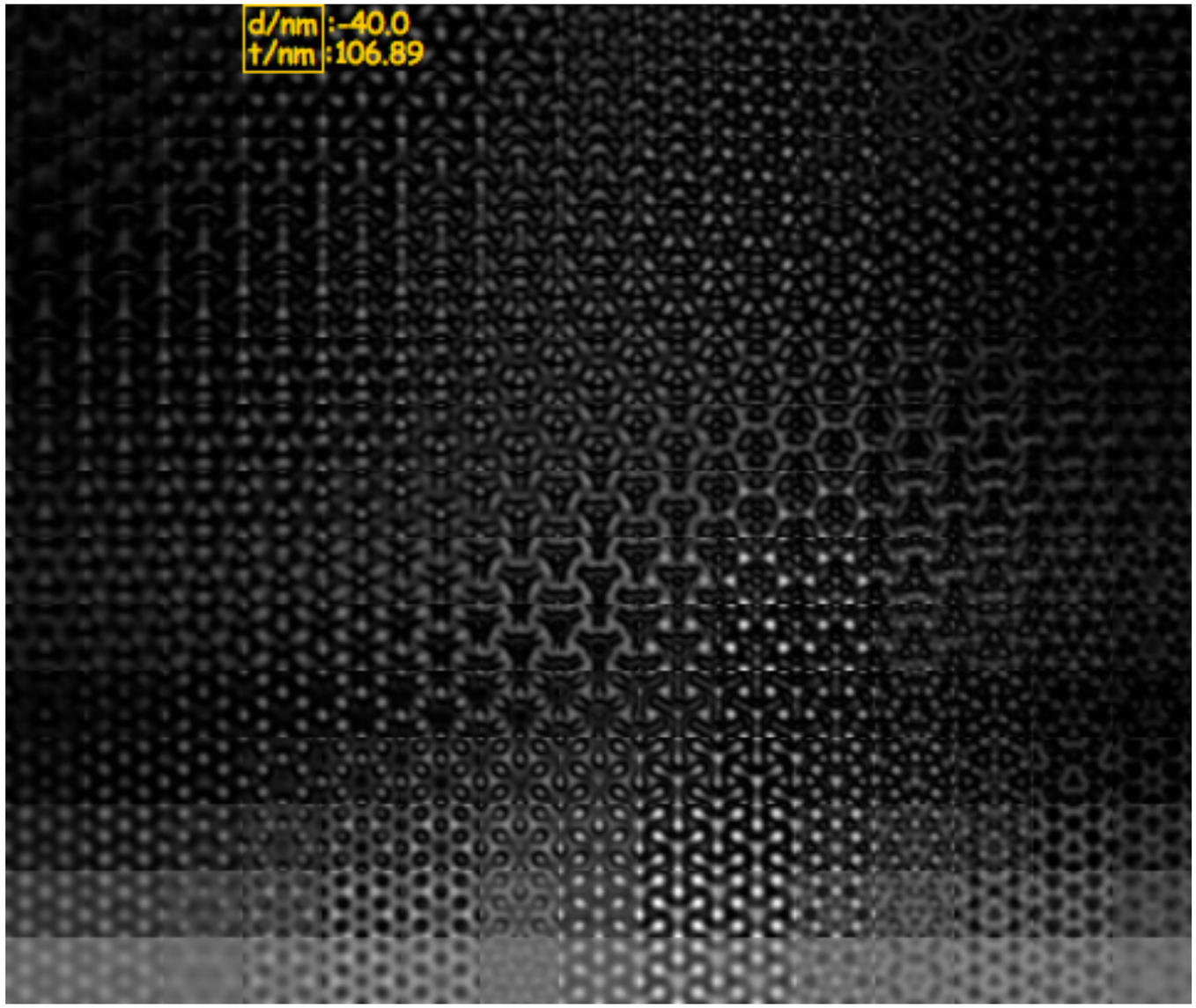

jEMS software

Needed:
crystal system (7), space group (230), lattice parameters, atoms (nature, x, y, z, occupancy)

jEMS → free access on TeamViewer PC at ScopeM

Multislice technique

Question:

How to define the diffraction condition ?

The beam direction is defined by the normal to the slices. This implies in most of the cases of molecular dynamics simulation that the beam direction is a low index crystallographic direction such as <001>, <011>, <111> or at most <112>:

Appropriate for **HREM** and atomic imaging.
Not so appropriate for **CTEM** imaging.

For CTEM it is more appropriate to image with a single systematic row, defined by one diffraction vector g. In order to attain such an imaging condition, a method was developed. It consists in tilting the specimen before slicing. This corresponds in fact to what the operator is doing on the microscope. The idea is to go away from the main zone axes, by about 10°, by a first tilt around the diffraction vector that will define the systematic row. To reach the desired weak beam condition, such as g(4g) it is still necessary to do a second tilt, perpendicular to the diffraction vector , of about 1°.

Multislice technique

- **Defining the diffraction condition**

First tilt:

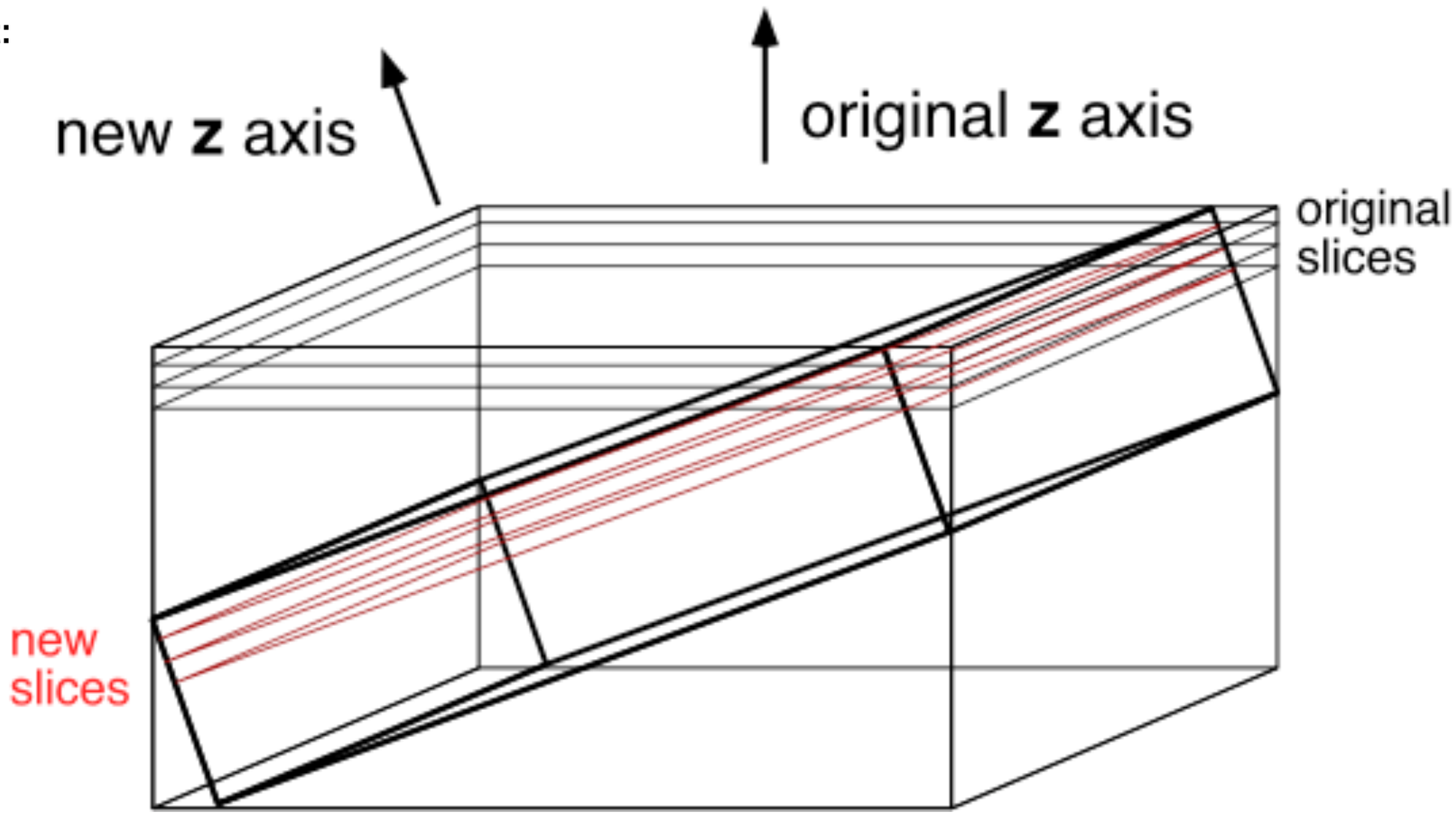

Multislice technique

- **Defining the diffraction condition**

Being based on (fast) Fourier transforms, the multislice technique requires periodic slices in x and y. Otherwise artificial contrasts enter in the image from the boundaries of the image, as if they were planar faults at the boundaries. While this condition is preserved in molecular dynamics samples calculated with periodic boundary conditions, this is not true anymore when this same specimen is tilted before slicing.

-> Slicing direction is selected in order to perserve periodicity, e.g. from [001] to [015]:

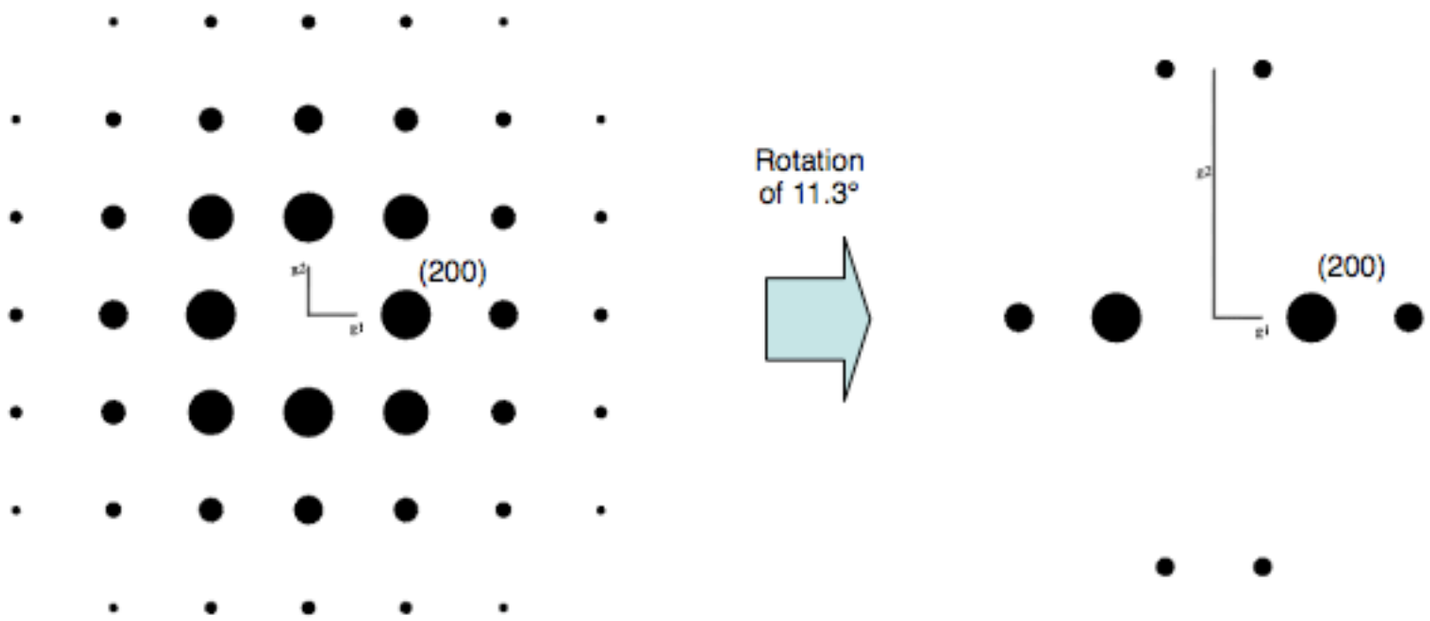

Multislice technique

- **Defining the diffraction condition**

Second tilt:

The second tilt is performed by shifting the slices by some Δx at every slice. This approximation is based on the fact that in each slice atomic positions, or scattering centres, are projected onto a 2D representation. The resulting projected potential is insensitive to differences in height of the atoms within one slice. The horizontal position however is slightly affected by a real tilt, but the difference is negligleable for angles in the 1° range.

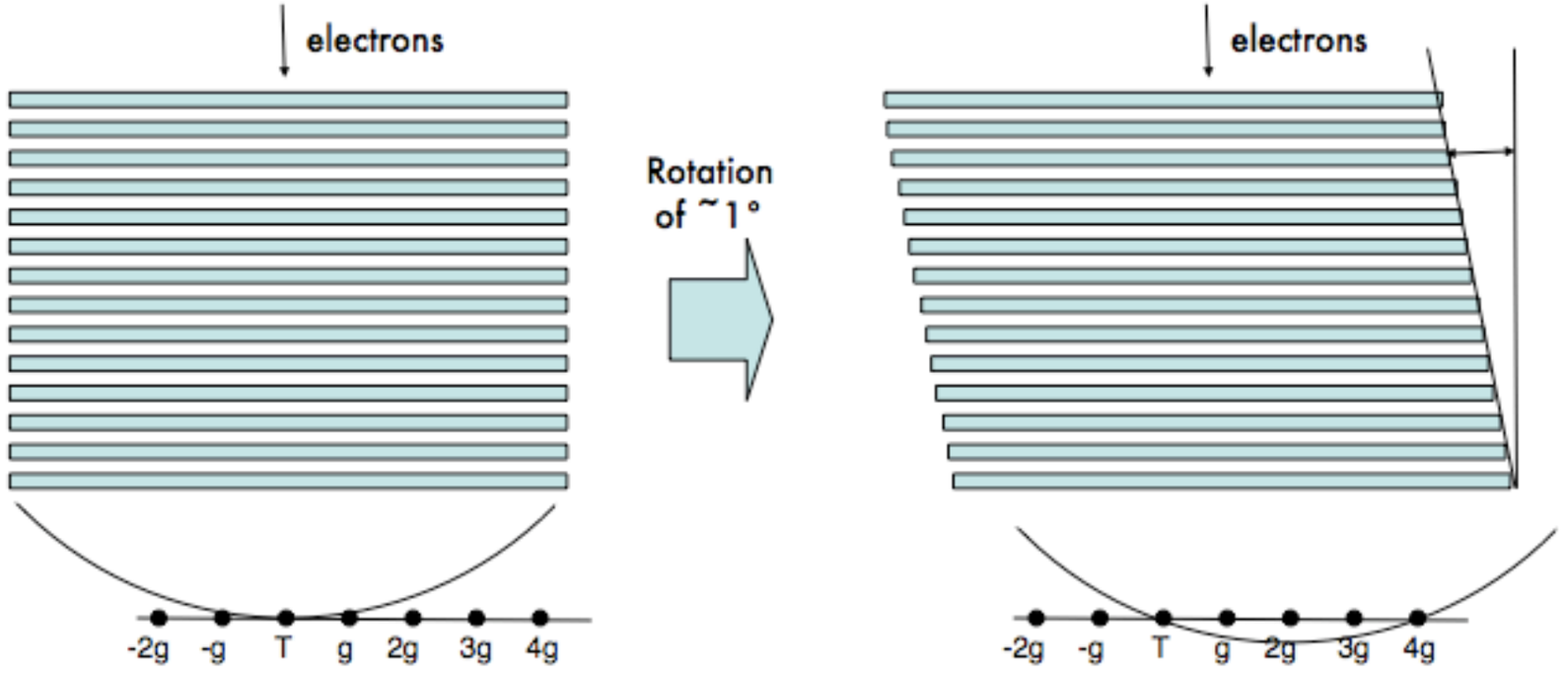

Multislice technique

Considerations on sample size and sampling

Sampling should allow for sufficient spatial resolution. It appears that a pixel size of about 0.1 Angstroem is sufficient. In practice this implies that to simulate the image of a molecular dynamics sample of, for example, 100'000 Al atoms in a cube, a sampling of 1024x1024 is appropriate. This results in a square image that is about 10 nm a side (with hence a spatial resolution of about 0.1 Angstroem).

Calculation time is also something to consider. The above example is calculated nowadays in about 1 day in a single processor machine. When a higher number of atoms is treated the calculation time increases for two reasons. The first is due to the calculation of the interaction of the electron wave with a larger number of scattering centres, and the second is due to the higher sampling, e.g. 2048x2048 or higher, needed because of the larger MD box.

3 to 4 millions atoms are manageable, including both the image simulation time and the handling of the image in image treatment softwares (PhotoShop® or other). This represents a cubic box with side of 40 nm, which is quite close to what is handled experimentally in a TEM, both in terms of sample thickness and image area.

Simulation techniques: many beam calculation or multislice technique ?

- Both have advantages and drawbacks, one has to carefully design the project before jumping onto them:

- Many beam calculation: complex data set, easy to run and fast
- Multislice technique: easy data set, complex to run and slow

Multislice calculation examples

The Frank loop-type cluster in Al

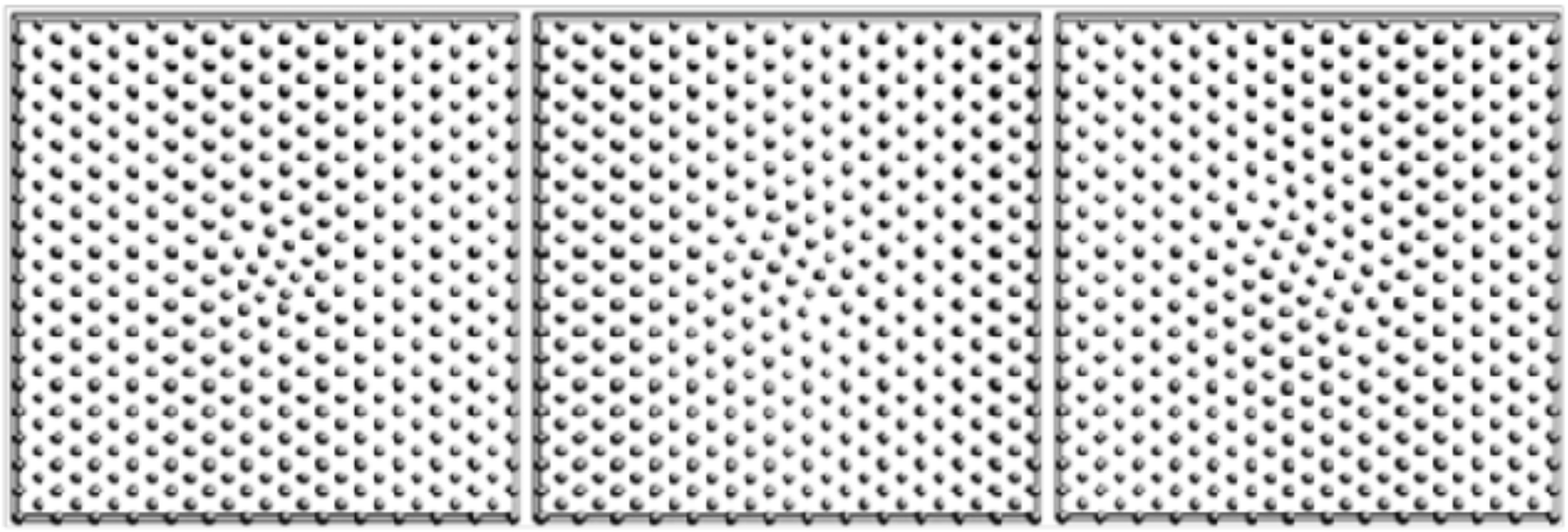

Interstitial Frank loop simulated TEM images using weak beam **g**(3.1**g**), **g**=(200) at 200 kV in Al for a diameter of about (a) 1.0 nm (8 interstitials), (b) 1.5 nm (19 interstitials) and (c) 2.0 nm (37 interstitials).

- Simulations indicate that **nanometric loop size is difficult to resolve below 2 nm**

The Frank loop-type cluster in Al

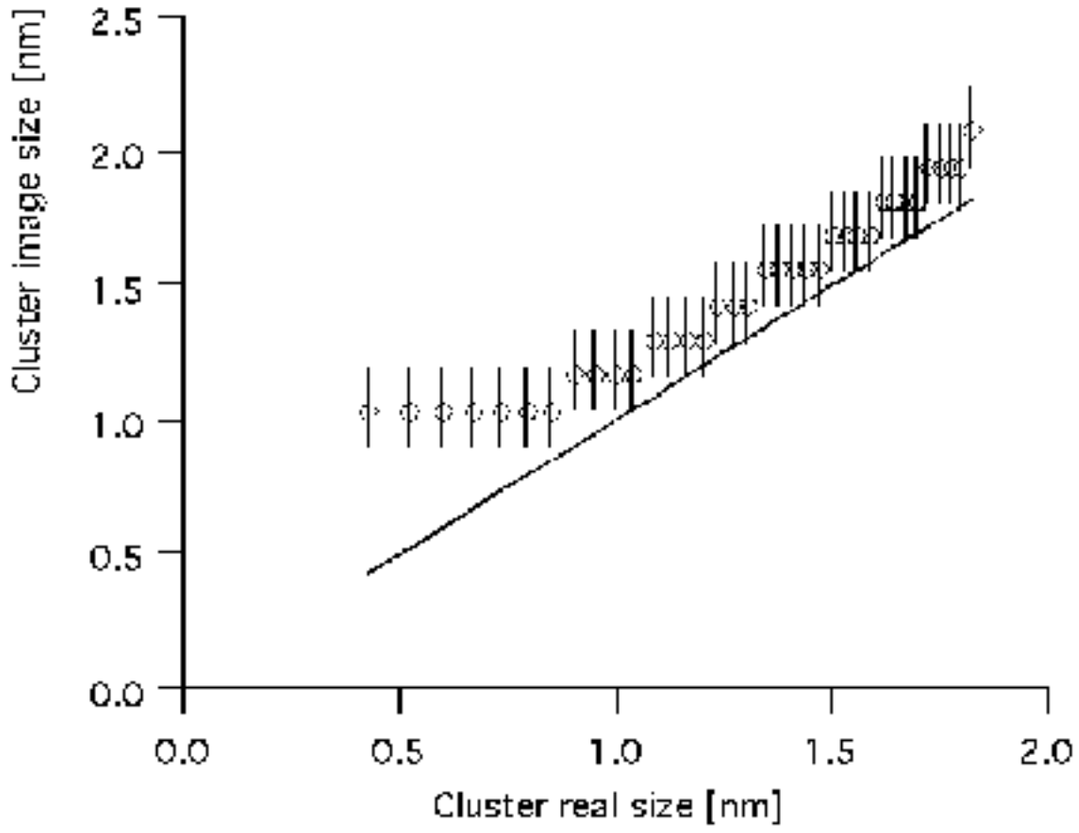

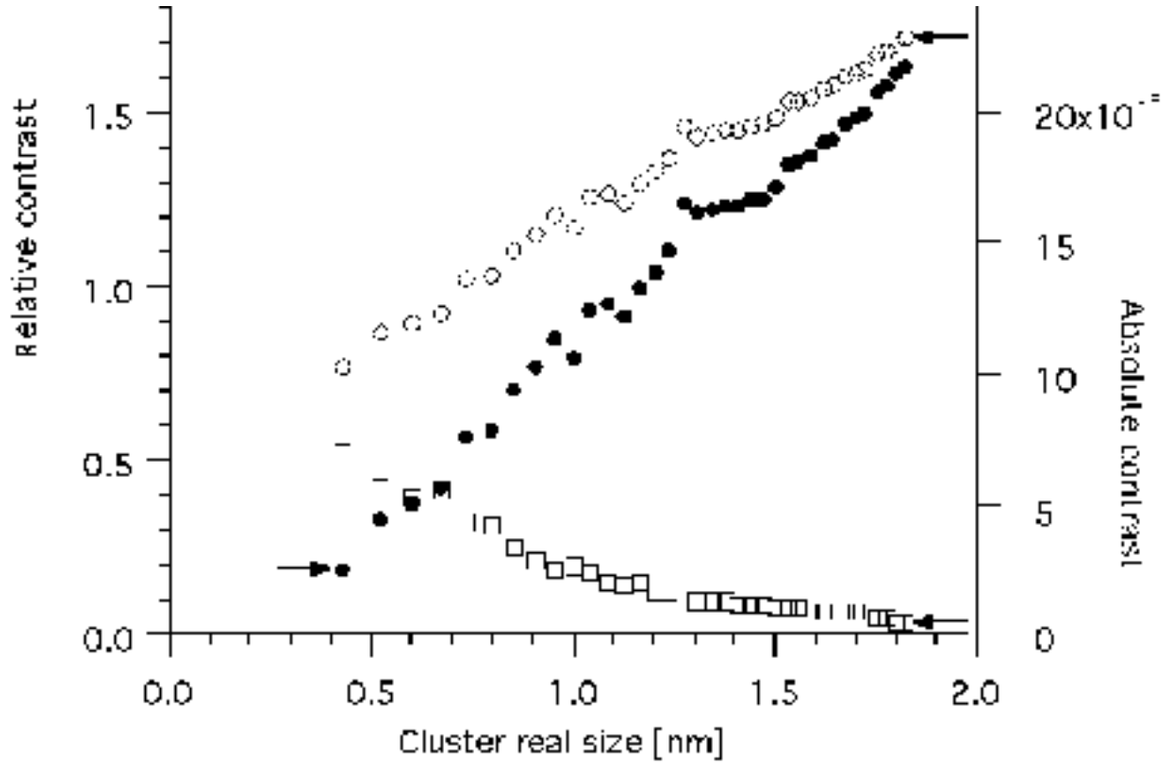

- Simulations indicate that **nanometric loop image size saturates < 1 nm**
- Simulations indicate that a **cluster of 2 interstitials has 20 % contrast**, enough to be seen experimentally, in principle ! (background noise is at best 10%)

R. Schaublin, A. Almazouzi, Y. Dai, Y. N. Osetsky and M. Victoria
Journal of Nuclear Materials 2000 Vol. 276 Pages 251-257

Large dislocation loops in ferritic steels

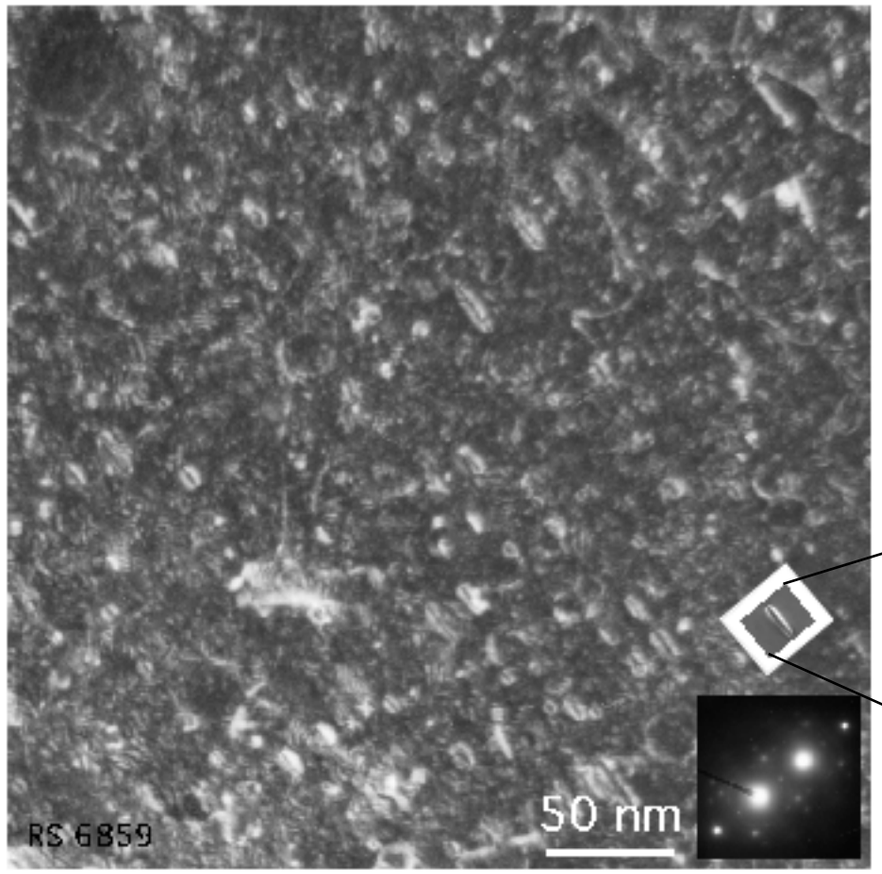

F82H, 8.8 dpa, Weak beam g(3.1g)
g=(200) 200 kV thickness ~60 nm

MD simulation

Interstitial loop in pure Fe
937 interstitial <100> loop
on (100) plane
Weak beam g(4.1g) g=(200)
200 kV
thickness 18 nm
Image width = 22.9 nm

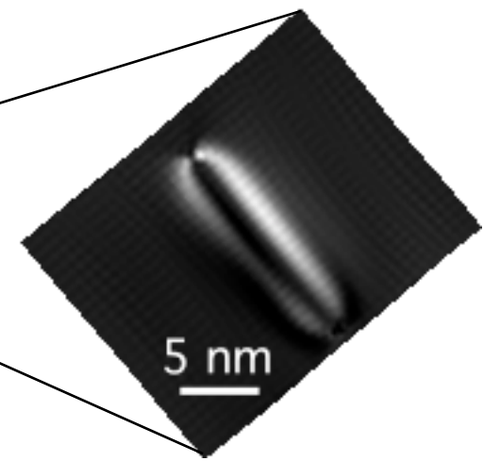

- **Good match between experimental and simulated image** of dislocation loop in steel
- **Allows raising ambiguity** on the **identification** of the loop's **Burgers vector**

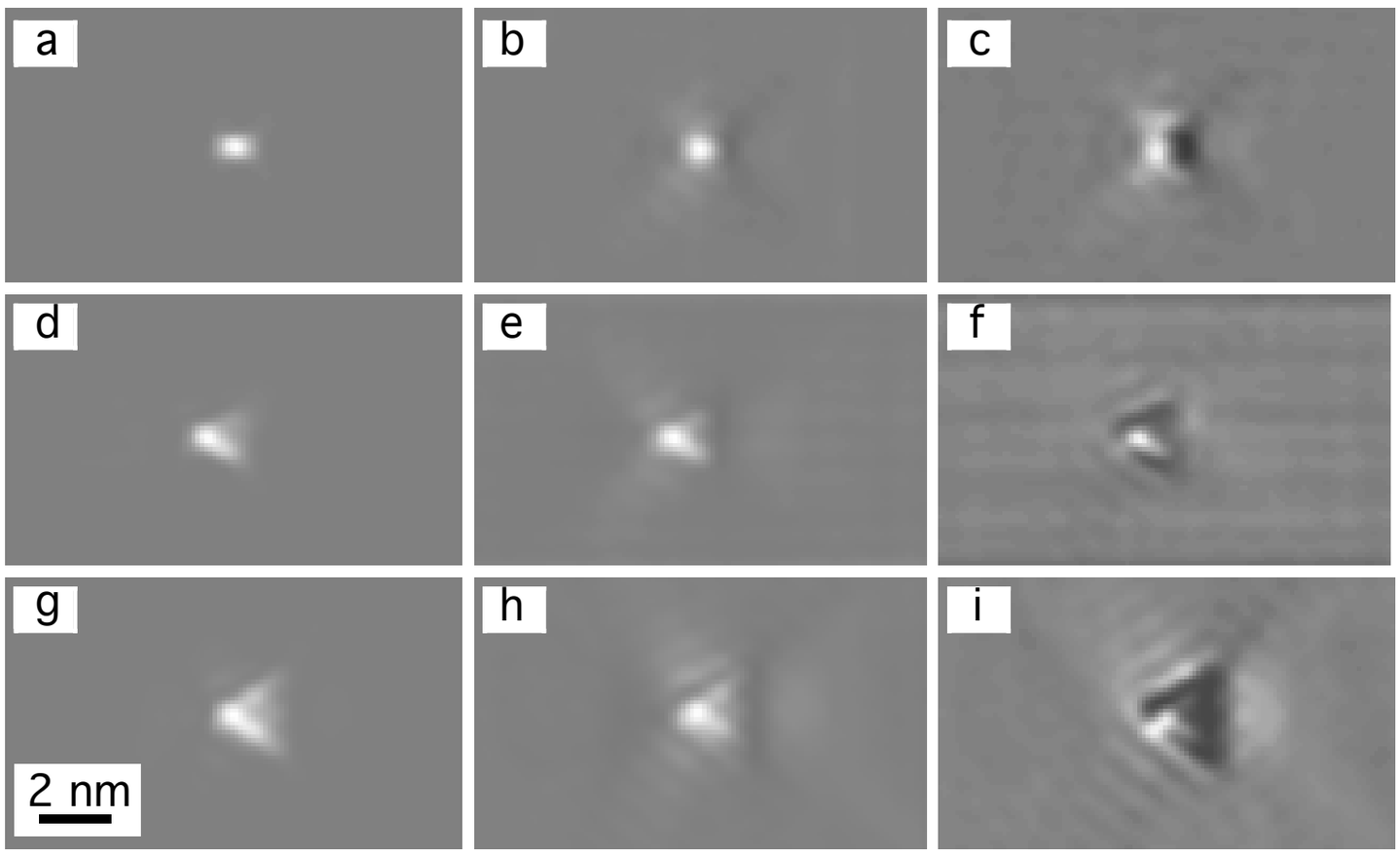

SFT simulated TEM images using weak beam **g**(6.1**g**), **g**=(200) at 200 kV in Cu as a function of SFT size and sample thickness. 21-vacancies SFT in a sample (a) 10.4 nm, (b) 11.6 nm and (c) 13.2 nm thick. 45-vacancies SFT in a sample (d) 13.6 nm, (e) 12.0 nm and (f) 15.2 nm thick. 91-vacancies SFT in a sample (g) 10.4 nm, (h) 11.6 nm and (i) 13.2 nm thick.

Simulations indicate that SFT's contrast in TEM is more complex that one generally assumes:

- **contrast** can **change from white to black**
- **SFTs below 2 nm look like loops ...**

R. Schaublin, A. Almazouzi, Y. Dai, Y. N. Osetsky and M. Victoria
Journal of Nuclear Materials 2000 Vol. 276 Pages 251-257

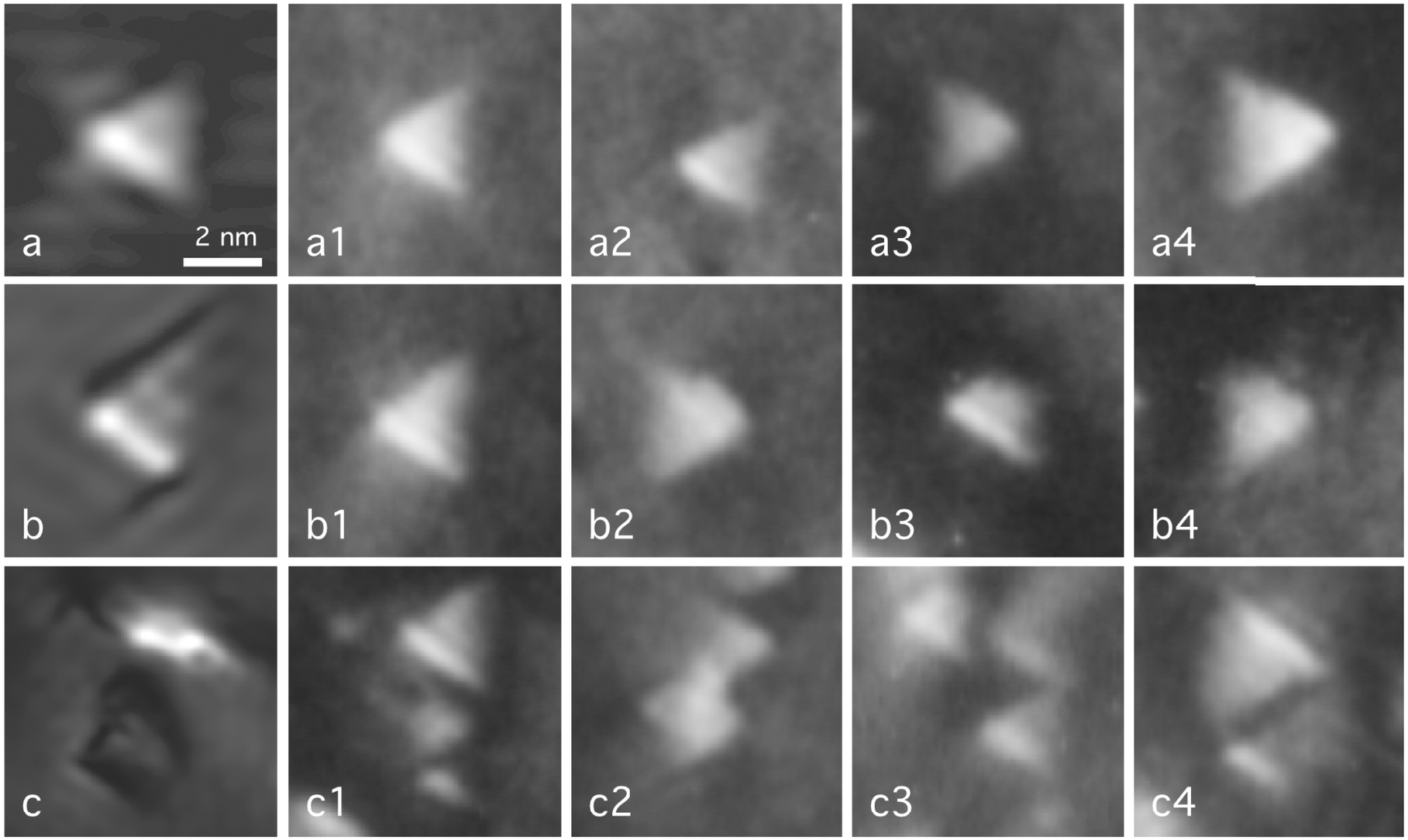

Table of TEM weak beam images in Cu irradiated at room temperature to 0.046 dpa, showing (row a) perfect SFTs, (row b) truncated SFTs and (row c) groups of intermixed SFT. First column of images (a, b and c) shows corresponding simulated images while second to fourth columns (a1-a4, b1-b4 and c1-c4) show corresponding typical experimental images of those.

- With simulations one can distinguish between perfect, truncated and intermixed SFTs

R. Schaublin, A. Almazouzi, Y. Dai, Y. N. Osetsky and M. Victoria
Journal of Nuclear Materials 2000 Vol. 276 Pages 251-257

Beat the diffraction limit !

ø20 μm

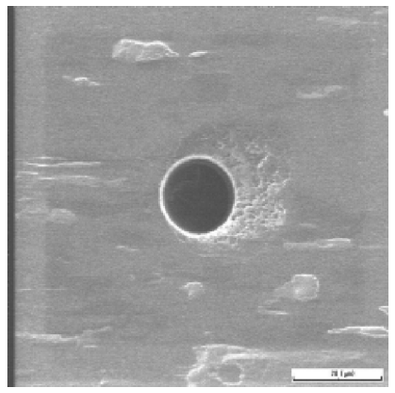

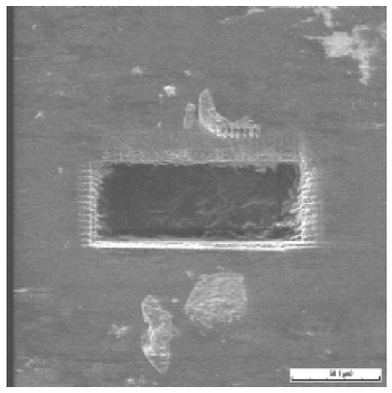

50x100 μm^2

Objective aperture

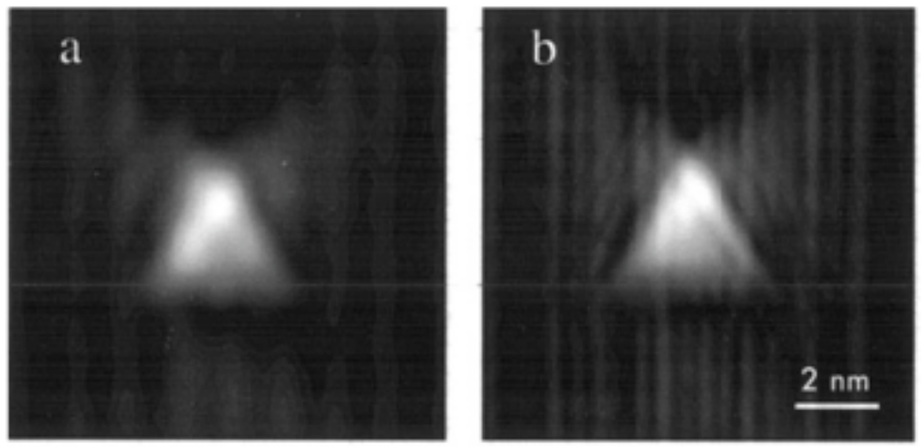

Simulation

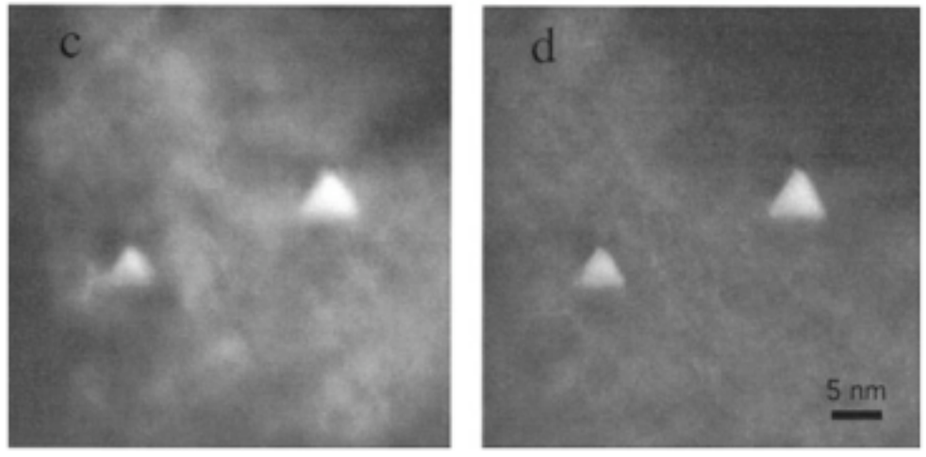

Experiment

Fig. 15. Simulated (**a** and **b**) and experimental (**c** and **d**) weak beam TEM images, 200 kV, **g**(6**g**), (**g**200), close to a zone axis <011>, of SFT, obtained with an objective aperture size of (a) 2.8 nm^{-1}, (b) 2.8 × 6.5 nm^{-2}, (c) ϕ 40 μm, and (d) 40 × 100 μm^2. Experimental images made in Au quenched in water from the melting temperature.

- Rectangular aperture: **gain in resolution** (6.5 Å down to 3.0 Å, theoretical)

Cavities in TEM: Fresnel contrast

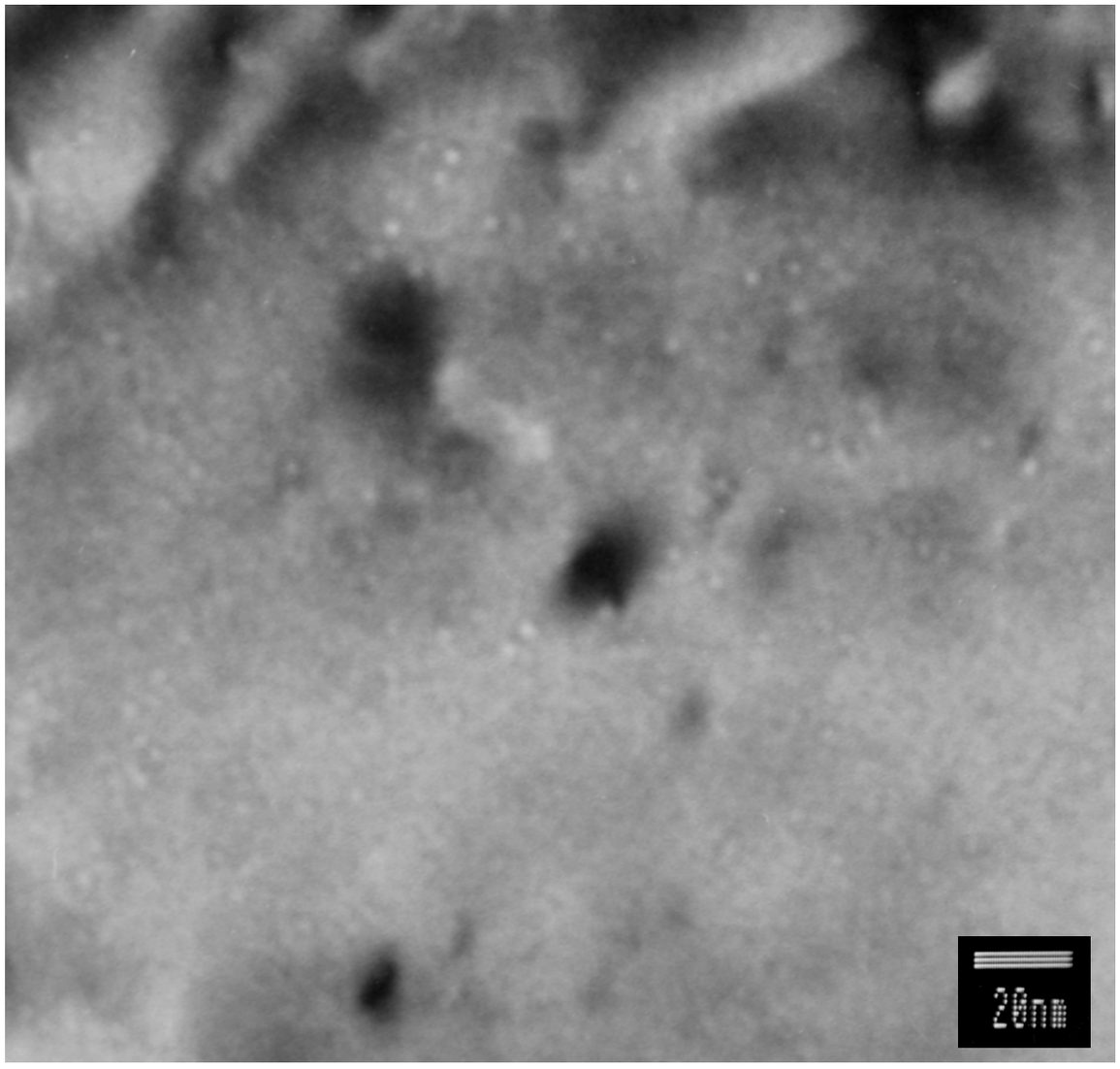

TEM investigation of cavities in irradiated F/M steel (F82H)

• **Cavities** appear as bright disks surrounded by a dark ring (**overfocused**) or vice-versa (**underfocused**).

high resolution TEM

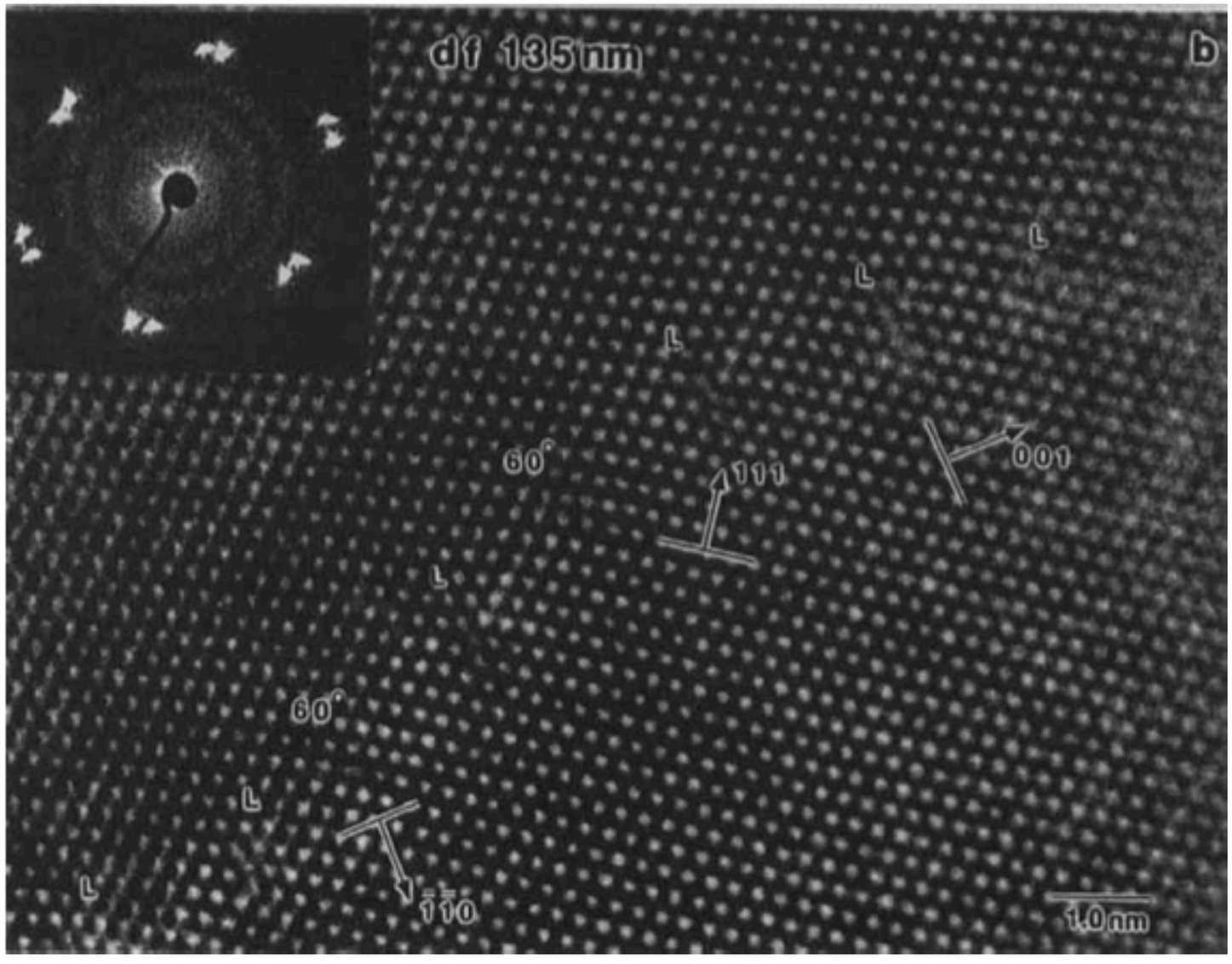

Dislocations in Al

Beware of image forces !
the **Eshelby twist :**

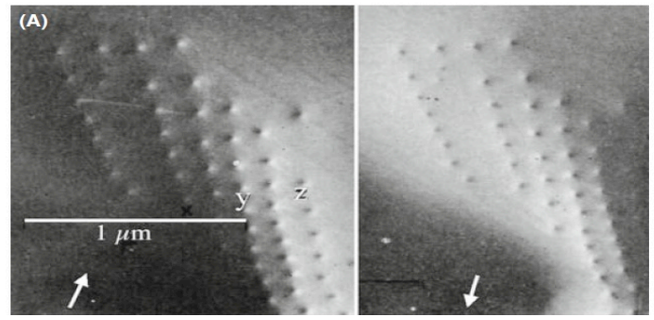

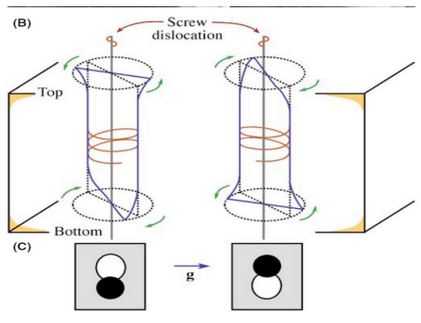

Problem: the required sample thinness has a strong impact on the defect configuration because of the **image forces** induced by the free surfaces

scanning TEM

weak beam 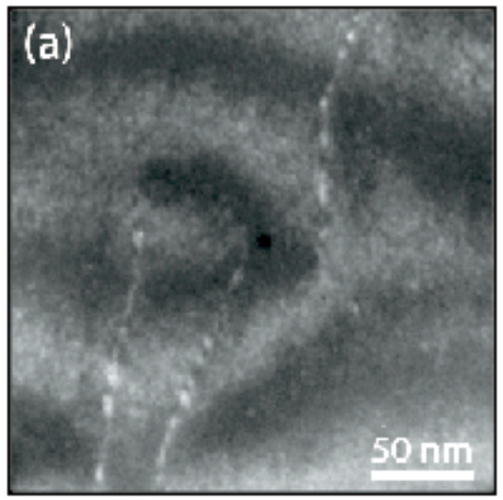

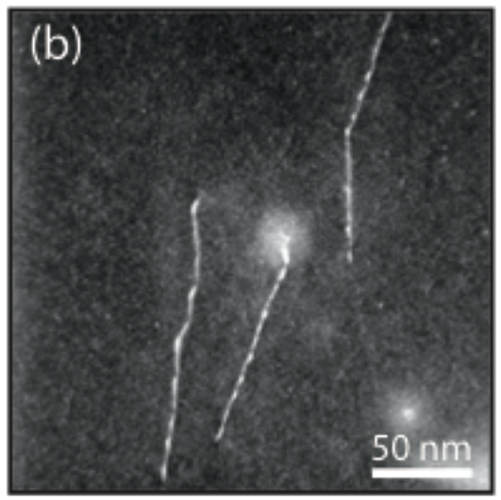

STEM

+ large convergence angle allows reducing thickness dependent contrast oscillation
- undefined diffraction condition (bad for e.g. g·b analysis)

Convergent weak beam technique : + defined diffraction condition / - demanding

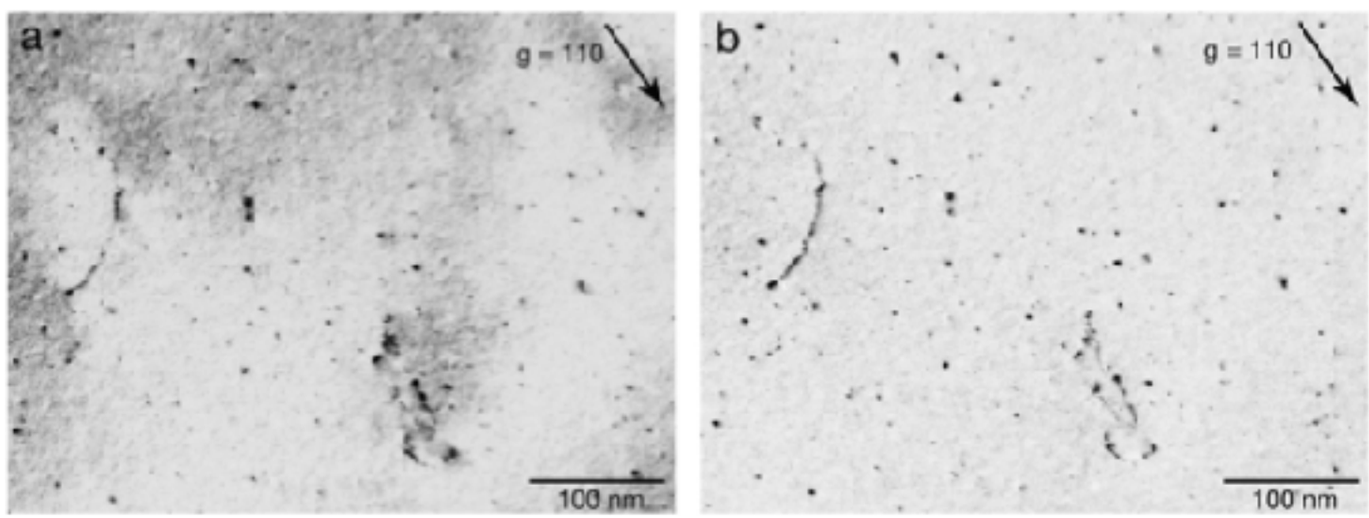

Fig. 3. Fe–10Cr irradiated at RT to 0.45 dpa with 500 keV Fe^+ and simultaneously implanted with 880 appm He. (a) WB micrograph taken under g(4g) diffraction condition, g = {011}; (b) same region captured using the CWBT with a series of diffraction conditions around g(4g). Micrographs are shown in inverted contrast.

Experimental validation of image forces

How to 'see' image forces ?
-> TEM on inclined screw dislocation in thin TEM sample of ultra high purity Fe
Anisotropic elastic field including image forces now implemented in CUFOUR code to simulate the TEM image of crystal defects (Schäublin *et al.* MSE A 1993)

b 1/2 a <111>, dislocation line <111>, g {110}, bright field, 200 kV (JEOL 2010, LaB6)
g·b = 0 observation condition (invisibility condition)

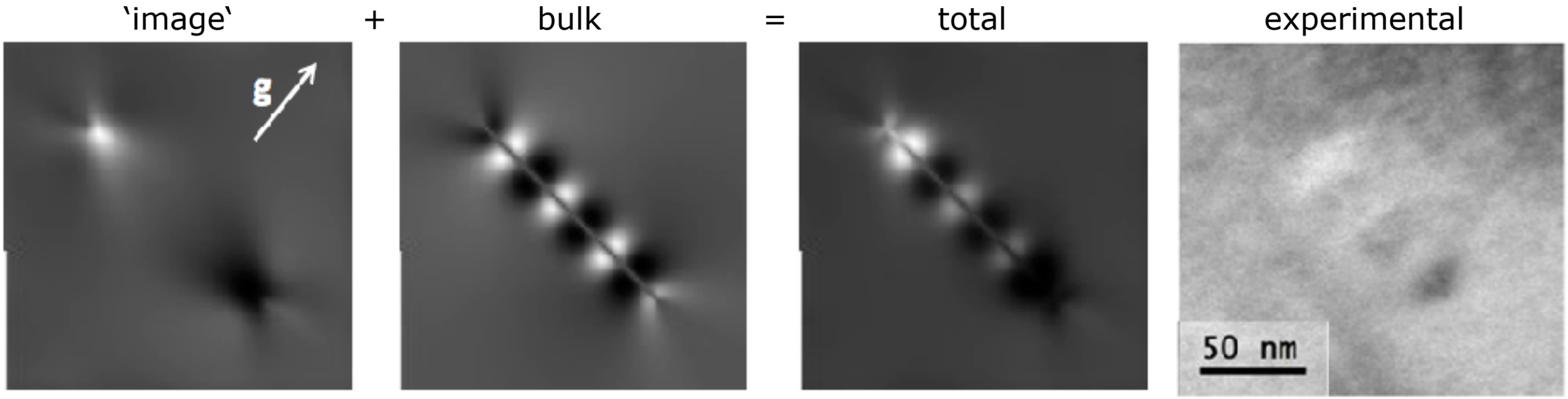

Wenwang Wu, EPFL, Switzerland, PhD thesis 2014

- There is a good qualitative match between 'total' image and experimental image
- The image stress effect is remarkable near the tips of inclined dislocation under invisibility condition, as the absolute amplitude of residual contrast is quite low (≤0.2), which is comparable to image stress induced contrast amplitude (also ≤0.2)

W.W. Wu, R. Schaublin, J.C. Chen, General dislocation image stress of anisotropic cubic thin film, Journal of Applied Physics 112(9) (2012) 093522
W.W. Wu, R. Schaublin, The elasticity of the 1/2 a_0 <111> and a_0 <100> dislocation loop in alpha-Fe thin foil, Journal of Nuclear Materials 510 (2018) 61-69
W.W. Wu, R. Schaublin, Simulations of weak-beam diffraction contrast images of dislocation loops by the many-beam Schaeublin-Stadelmann equations, Journal of Materials Science 53 (22) (2018) 15694-15702

References

C.T. Forwood and L.M. Clarebrough, “Electron Microscopy of Interfaces in Metals and Alloys”, Adam Hilger Ed., Bristol, Philadelphia and New York, 1991.

A.K. Head, P. Humble, L.M. Clarebrough, A.J. Morton and C.T. Forwood, “Computed Electron Micrographs and Defect Identification”, North-Holland Publishing Company, Amsterdam, 1973.

P.B. Hirsch, A. Howie, R.B. Nicholson, D.W. Pashley and M.J. Whelan, “Electron Microscopy of Thin Crystals”, London, 1969.

R. Schäublin R. and P. Stadelmann, "A method for simulating electron microscope dislocation images", Materials Science and Engineering, A 164 (1993) 373-378.

P.A. Stadelmann, "EMS – A software package for electron diffraction analysis and HREM image simulation in materials science", Ultramicroscopy, 21 (1987) 131-146.

E.J. Kirland, “Advanced Computing in Electron Microscopy”, Springer Science and Business Media, 1998.

D.B. William, C.B. Carter, “Transmission Electron Microscopy”, Springer Science and Business Media, 2009.

J. W. Edington, “Interpretation of transmission electron micrographs”, Philips Gloeilampenfabrieken, Eindhoven, 1975.

M. J. Mills and P. A. Stadelmann. “A study of the structure of lomer and 60 degree dislocations in aluminium using high-resolution transmission electron microscopy”, Phil. Mag., 60 (1989) 355-384

R. Schäublin, P. de Almeida, A. Almazouzi, M. Victoria, “Correlation Of TEM Images With Irradiation Induced Damage”, Journal of Nuclear Materials, 283-287 (2000) 205-209

R. Schäublin, “Nanometric crystal defects in transmission electron microscopy”, Microscopy Research and Technique, 69 (5) (2006) 305-316

Thank you for your attention
and best wishes